Received: 3 April 2023 | Revised: 15 September 2023 | Accepted: 30 September 2023

DOI: 10.1002/aoc.7293

RESEARCH ARTICLE

Applied Organometallic Chemistry WILEY

# Green synthesized AgNPs, CuONPs, and Ag-CuO NCs to effective antibiofilm activities and their potential application in aquaculture

**Dinesh Babu Manikandan**[1] | **Manikandan Arumugam**[1] | **Ubais Abdul**[1] | **Arun Sridhar**[1,2] | **Zulhisyam Abdul Kari**[3,4] | **Guillermo Téllez-Isaías**[5] | **Thirumurugan Ramasamy**[1]

[1]Laboratory of Aquabiotics/Nanoscience, Department of Animal Science, School of Life Sciences, Bharathidasan University, Tiruchirappalli, Tamil Nadu, India

[2]Immunology-Vaccinology, Department of Infectious and Parasitic Diseases, Fundamental and Applied Research for Animals & Health (FARAH), Faculty of Veterinary Medicine, University of Liège, Liège, Belgium

[3]Department of Agricultural Sciences, Faculty of Agro-Based Industry, Universiti Malaysia Kelantan, Jeli Campus, Jeli, Malaysia

[4]Advanced Livestock and Aquaculture Research Group, Faculty of Agro-Based Industry, Universiti Malaysia Kelantan, Jeli Campus, Jeli, Malaysia

[5]Department of Poultry Science, University of Arkansas, Fayetteville, Arkansas, USA

**Correspondence**
Thirumurugan Ramasamy, Laboratory of Aquabiotics/Nanoscience, Department of Animal Science, School of Life Sciences, Bharathidasan University, Tiruchirappalli 620 024, Tamil Nadu, India.
Email: ramthiru72@bdu.ac.in

**Present address**
Arun Sridhar, Immunology-Vaccinology, Department of Infectious and Parasitic Diseases, Fundamental and Applied Research for Animals & Health (FARAH), Faculty of Veterinary Medicine, University of Liège, Liège, Belgium.

**Funding information**
This research received no external funding. The APC was funded by USDA-NIFA Sustainable Agriculture Systems Grant, Title of project: "Empowering US Broiler Production for Transformation and Sustainability USDA-NIFA (Sustainable Agriculture Systems)" (2019-69012-29905).

The expanded emergence of drug-resistant microbes remains a concern to the scientific community in developing effective therapeutics. Approach of green chemistry based nanomaterials fabrication is in high demand, due to biocompatibility, non-toxic, and high surface area that adheres more biomolecules on surface. Green fabricated silver nanoparticles (AgNPs), copper oxide nanoparticles (CuONPs), and silver–copper oxide nanocomposites (Ag-CuO NCs) were characterized by fluorescence and Raman spectroscopy, field emission scanning electron microscopy (FE-SEM) with energy-dispersive X-ray spectroscopy (EDX), and thermogravimetric (TG)/differential scanning calorimetry (DSC) analysis. Antibiofilm potential of green fabricated AgNPs, CuONPs, and Ag-CuO NCs was tested against aquatic pathogenic microorganisms such as *Aeromonas hydrophila*, *Pseudomonas aeruginosa*, and *Staphylococcus aureus*. This present study deals with bacterial growth rate, biofilm inhibition, and antibiofilm architecture of AgNPs, CuONPs, and Ag-CuO NCs under the visualization of confocal laser scanning electron microscopy (CLSM). The FE-SEM technique was used to observe dense and compact structure (control without NPs treatment) with treatment of NPs that showed reduced amount of cell population in *A. hydrophila*, *P. aeruginosa*, and *S. aureus*. The effective antibiofilm inhibition of Ag-CuO NCs was achieved by reducing micro-colonies compared with AgNPs and CuONPs. The AgNPs, CuONPs, and Ag-CuO NCs

demonstrated antibiofilm properties against Gram-negative and Gram-positive bacteria, indicating a combinatorial effect of green fabricated NPs in combination with plant metabolites against pathogenic bacteria. As a result, aforementioned nano-product merits further investigation in order to be used as a potent adjuvant therapy as antagonistic toward various bacterial diseases in aquaculture.

**KEYWORDS**

antibiofilm, drug resistance microbes, green fabrication, growth rate, nanoparticles

## 1 | INTRODUCTION

Nanotechnology is a multidisciplinary research concerned with the fabrication of nanoparticles (NPs) size smaller than 100 nm.[1] Production of NPs receives increasing attention and rising their demands, which can be established in all needs of human life such as food, cosmetics, energy, and household chemicals.[2] Green synthesized nanomaterials have advantageous physicochemical properties, due to its high stability, surface atoms' large proportion, spatial confinement, and key basis of phytochemical constituents that play a vital for the fabrication of NPs.[3] The nanomaterials have diverse applications in the field of biology, medicine, and material science.[4]

Silver nanoparticles (AgNPs) have been widely utilized as an antimicrobial therapeutic regime against variety of pathogenic microorganisms.[5] The AgNPs are used in cosmetics as well as in medicinal implants because of their optical, catalytic, and electrical properties.[6] The AgNPs are well known for its antimicrobial properties through various mechanistic functions such as enzymatic inactivation, oxidative stress, intracellular biomolecules, cell wall and membrane damage, etc.[7] Copper is an essential trace elements for living beings, but they can be applied in food, cosmetic products, and act as antifouling agent.[8] Silver–copper oxide nanocomposites (Ag-CuO NCs) have enormous potential due to their optical, electrical conductive, photoconductive, and bactericidal properties.[9] Utilization of binary metal nanocomposites rather than monometallic systems would also allow for the expansion of application fields.[10] In green chemistry approach, the silver and copper oxide NPs fabricated using plant-based extracts, which can be attributed as surface capping and stabilizing agent.[11] The secondary metabolites derived from plants such as sterols, phenolic compounds, alkaloids, flavonoids, and glycosides involve in reducing metal ions and convert into NPs. These natural metabolites have unique distinct biological activities, minimizing harmful effects, and explore in the development of long-term eco-friendly nanomaterials.[12] The life-threatening deleterious impact of bacterial biofilm formation mostly in therapeutic regime is a serious concern in clinical practice, particularly while treating chronic infections.[13] The prevalence of bacteria must be resolved by taking measures that concentrate not only just treating bacteria but also minimize pathogens' ability to form biofilms.

The aquaculture system is affected by different ways such as poor water quality, temperature increase, overcrowding, and waste/by-products disposal problems. These factors have an impact on the aquatic environment, resulting in the emergence of a variety of opportunistic pathogens. Bacterial disease exhibits major economic loss in the aquaculture farms.[14] The second most serious public health concern is infectious disease, with bacterial infections accounting for 12% of deaths globally.[15] Many studies have been emerged as a result of bacterial resistance to multiple antibiotics.[16] Antibiotics have difficulty in eliminating bacteria in chronic illnesses due to a shift in bacterial growth mode from free-swimming planktonic cells to motile society-organized biofilms.[17] *Pseudomonas aeruginosa* and *Staphylococcus aureus* are biofilm producing pathogenic microorganisms. The perseverance of infectious diseases is due to their ability to form biofilms and cause high rates of mortality as well as the challenges associated with biofilm formation control.[18] *S. aureus* is a Gram-negative bacterium that is associated with human opportunistic commensal pathogen. In global, *S. aureus* cause various infections and increase mortality rate.[19] Researchers have focused their attention on *P. aeruginosa*, because it is an opportunistic human pathogen and major cause of nosocomial infection, diffused panbronchiolitis, immunocompromised cystic fibrosis, and chronic obstructive pulmonary infection.[20]

In aquaculture industry, *Aeromonas hydrophila* infections cause hemorrhagic septicemia, which results to significant economic loss.[21] This emerging pathogen leads to severe health complications such as meningitis,

septicemia, wound infections, and gastroenteritis in immunocompromised patients all over the world.[22] Biofilms produced by microbial consortium formed on organ surfaces required for survival benefits such as attempting to evade host immune responses through altered expression of polysaccharide matrix and phagocytosis-resistant characteristics.[23] The quorum sensing attitudes of the microbial population combined with the expansion of multidrug-resistant (MDR) features create difficulty in treating hosts. Bacteria can form biofilms approximately 65% of microbial infections in the body.[24] Conventional antibiotic therapy for *P. aeruginosa*, *S. aureus*, and *A. hydrophila* are difficult, due to the development of biofilm with exopolysaccharide (EPS) production.[25] The microorganisms are resistant to antibiotics, and it has been a challenging task for prophylactic measures.[26] Hence, there is an urgent requirement to establish therapeutic spectrum against pathogenic microorganisms and control the emergence of highly virulent strains as a result of the excessive antibiotic use. The present research, green fabrication of silver nanoparticles (AgNPs), copper oxide nanoparticles (CuONPs), and silver–copper nanocomposites (Ag-CuO NCs) using *Ocimum americanum* L. aqueous leaf extract as surface capping and stabilizing agent. Green fabricated AgNPs, CuONPs, and Ag-CuO NCs were characterized by fluorescence and Raman spectroscopy, FE-SEM coupled with energy-dispersive X-ray spectroscopy (EDX), and TGA/DSC analysis. Furthermore, the green synthesized nanomaterials were evaluated as their use of potential antimicrobial agent against pathogenic microorganisms.

## 2 | MATERIALS AND METHODS

### 2.1 | Fabrication of nanomaterials

The *O. americanum* L. leaves were collected from Bharathidasan University, Tiruchirappalli, Tamil Nadu, India. The leaves of *O. americanum* were washed two to three times in running tap water to remove dust and other deposits. In detail, the collected leaves were shade-dried for 3 days at room temperature followed by grinding to make fine powder. The 5 g of leaf powder was boiled for 10 min in 50 mL of sterile distilled water. The preparation was filtered through Whatman no. 1 filter paper, and the extract was used for further studies. For the fabrication of AgNPs, 2 mL of aqueous leaf extract was added in a dropwise manner to 100 mL of 1 mM concentration of silver nitrate ($AgNO_3$) solution at room temperature (27°C ± 2°C) and incubated overnight. The aqueous leaf extract mixed with the $AgNO_3$ solution was subjected to water bath at 70°C. The color change of silver nitrate solution from yellowish white to dark brown indicated the formation of AgNPs. Finally, the samples were centrifuged at 6000 rpm for 15 min. After centrifugation, the organic moieties were removed, and the pellet was washed with ethanol. The powder form of NPs were air-dried in oven at 60°C and kept at 4°C for further analysis.[27] For the fabrication of CuONPs, 2 mL of aqueous leaf extract and 100 mL of 1 mM $CuSO_4{\cdot}5H_2O$ solution were mixed in a beaker. The colloidal solution was heated and stirred continuously at 80°C for 2 h. The color change confirmed the reduction process. In addition to this, the solution was repeatedly centrifuged at 6000 rpm, and collected pellets rinsed with distilled water, then the obtained particles were air dried in oven at 60°C. Consequently, the particles were grounded and processed at 4°C for further studies.[28] Equal volume of green fabricated AgNPs and CuONPs were mixed to allow complete reduction and formation of Ag-CuO NCs by vigorous stirring and centrifuge at 7500 rpm for 15 min. After centrifugation, elimination of other impurities and the particles were done by distilled water washing followed by ethanol, and the collected particles were air dried in an oven at 60°C for further studies.[29]

### 2.2 | Physicochemical characterization

Green fabricated AgNPs, CuONPs, and Ag-CuO NCs were characterized by fluorescence spectroscopy (Horiba, TCSPC) in which fluorescence emission spectra of AgNPs, CuONPs, and Ag-CuO NCs were recorded in the range of 375–440 nm, 405–445 nm, and 385–445 nm at an excitation wavelength of 270, 300, and 280 nm, respectively. The monochromatic radiation emitted by the He–Ne laser (633 nm), functioning at 20 mW was used to measure the green fabricated AgNPs, CuONPs, and Ag-CuO NCs analyzed by Raman spectroscopy HR 800 (Jobin Yvon, Horiba, France) and FE-SEM with EDX analysis to find out the surface topology and elemental composition of the respective NPs (FE-SEM, Carl Zeiss, UK). The thermal behavior of the green fabricated AgNPs, CuONPs, and Ag-CuO NCs was evaluated using TGA/DSC equipment (STA 300, Hitachi, Tokyo, Japan) under high temperature up to 700°C at a heating rate of 15°C/min.

### 2.3 | Bacterial strain

The bacterial isolates used were Gram-negative: *A. hydrophila* (MTCC 646), *P. aeruginosa* (MTCC 2488), and Gram-positive: *S. aureus* (MTCC 96). The bacteria were incubated at 28°C for 14 h on a Luria-Bertani (LB) plate; single colonies were picked, inoculated into liquid LB

medium, and further incubated at 37°C for 14 h. The bacterial cells were harvested by centrifugation at 5000 rpm for 10 min, and the collected pellets were resuspended in phosphate-buffered saline (PBS) and diluted to obtain the required concentration ($2 \times 10^7$ CFU/mL).

## 2.4 | Bacterial growth rate

The growth rate analysis of *A. hydrophila*, *P. aeruginosa*, and *S. aureus* in the presence of green fabricated AgNPs, CuONPs, and hybrid Ag-CuO NCs were investigated at different concentration (10–100 μg/mL) followed by the method of Dheilly et al.[30] Briefly, 10 μL of inoculum was taken from bacterial suspensions ($10^6$ CFU/mL suspensions) and added to the 96-well microtiter plate containing varying concentration of respective nanomaterials. The plates were incubated at 37°C and the growth rate was measured using ultraviolet–visible (UV–Vis) spectrophotometer at 600 nm at 4 h intervals up to 24 h. The assay was performed in triplicates.

## 2.5 | Biofilm formation assay

The AgNPs, CuONPs, and hybrid Ag-CuO NCs were used for the estimation of antibiofilm formation as adopted method of Cassat et al.[31] The antibiofilm activity of *A. hydrophila, P. aeruginosa*, and *S. aureus* in the presence of green fabricated AgNPs, CuONPs, and hybrid Ag-CuO NCs were determined at different concentrations (10, 50, and 100 μg/mL). The overnight incubated microorganisms were transferred to LB broth and adjusted to OD 600 of 0.1 ($10^6$ CFU/mL suspensions). Aliquots of the suspension (100 μL) was added into 96-well flat-bottomed polystyrene plate and incubated at 37°C for 48 h. After incubation, the plates were washed thrice with 1× PBS (pH 7.4), and the adherent cells were treated with 0.1% crystal violet staining for 10 min and further solubilized by 95% ethanol and then measured the optical density (OD) observed at 590 nm. The experiment was performed in triplicates, and the mean biofilm of absorbance value was used to assess the biofilm forming capacity of the strain. The following formula was employed to determine the percentage of biofilm inhibition in all treated wells compared to the untreated negative control and positive control (streptomycin):

$$\text{Biofilm inhibition}(\%) = \frac{\text{OD of untreated control} - \text{OD of treated sample x100}}{\text{OD of untreated control}}$$

## 2.6 | Confocal laser scanning microscopic analysis

Biofilms were grown on glass slides (1 × 1 cm) in 24-well polystyrene plates supplemented with the concentration (100 μg/mL) of AgNPs, CuONPs, and hybrid Ag-CuO NCs. The cultures were incubated for 24 h at 37°C, and they were subjected to washing thrice with 0.1 M PBS (pH 7.4) to eliminate non-adherent *A. hydrophila*, *P. aeruginosa*, and *S. aureus* cells followed by staining with 0.1% acridine orange/ethidium bromide (AO/EB) fluorescent staining solution. The excessive stain was eliminated, and the slides were air-dried before examination. Cells grown in the glass slides with untreated cells (negative control), with streptomycin as positive control, were compared with AgNPs, CuONPs, and Ag-CuO NCs. Stained slides were visualized under confocal laser scanning microscope (CLSM; Model LSM 710, Carl Zeiss, Germany) and processed with Zeiss LSM Image Examiner (Version 4.2.0.121), equipped with an excitation filter (515–560 nm). CLSM images (50×) were obtained from untreated control and treated biofilms. Mean and maximum thickness of biofilms formed on the glass surface was estimated by Z-stack analysis.

## 2.7 | FE-SEM imaging

The field emission scanning electron microscope (FE-SEM) (Carl Zeiss, UK) was used to assess the antibiofilm activity of green synthesized AgNPs, CuONPs, and hybrid Ag-CuO NCs tested against *A. hydrophila*, *P. aeruginosa*, and *S. aureus*. Biofilms were grown on silicon substrate (1 × 1 cm) in 24-well polystyrene plates supplemented with 100 μg/mL of AgNPs, CuONPs, and hybrid Ag-CuO NCs. The bacterial cultures were incubated for 24 h at 37°C. After the incubation period, the cells were washed three times with 0.1 M PBS (pH 7.4) to eliminate non-adherent *A. hydrophila*, *P. aeruginosa*, and *S. aureus* cells. The bacterial cells were grown over the silicon substrate. The surface adhered bacterial cells were fixed with 2.5% of glutaraldehyde and kept at 4°C for 5 h. Further, the air-dried silicon substrate was washed twice with varied concentration of alcohol (25%, 50%, 75%, and 100%) for each 10 min, and it was kept at overnight incubation. Then, the respective samples were subjected to gold sputter-coated with surface in a 3 nm thickness.

### 2.8 | Statistical analyses

All the data were expressed as mean ± standard deviation (SD) of the triplicates. The values of triplicates were compared using two-way analysis of variance (ANOVA) followed by Duncan's multiple range test (DMRT) as post-hoc analysis in SPSS 16.0 (SPSS inv., Chicago, IL, USA) and Dunnett's multiple comparison test using GraphPad Prism 8 software. *, **, *** and **** indicate significant difference of $p$-value ≤0.05, 0.01, <0.001, and 0.0001, respectively. All graphs were rendered by graphical software (OriginPro 9.0).

## 3 | RESULTS AND DISCUSSION

### 3.1 | Physicochemical characterization

Generally, the synthesis of NPs was initially confirmed by UV–Vis spectroscopy techniques, due to the surface plasmon resonance (SPR) effect observed at specific wavelengths (200–800 nm). The AgNPs absorbance wavelength ranges between 400 and 500 nm, and the CuONPs absorbance wavelength ranges from 300 and 400 nm. The green synthesized AgNPs showed sharp absorbance peak at 425 nm,[27] and the CuONPs was sharp SPR peak appeared at 360.74 nm.[28] However, the similar findings were reported that the AgNPs synthesized using *Phoenix dactylifera* seed extract showed peak at 420 nm and the rapid green synthesized CuONPs showed two peaks at 233 and 367 nm.[31] Dynamic light scattering (DLS) analysis was used to measure the size distribution of the green synthesized AgNPs, CuONPs, and Ag-CuO NCs. The average size distribution of the green synthesized AgNPs, CuONPs, and Ag-CuO NCs was 48.25, 330.5, and 69.80 nm, respectively. The NPs have higher surface area and smaller size, which increases their biological reactivity.[32] The NPs size plays a crucial role for biological distribution, and the smaller-size NPs can easily penetrate the cell wall membrane. The bioreactivity of the smaller-size NPs has increased penetration into the cell wall membrane, deactivating metabolic and enzymatic dysfunctions.[33] The smaller size of NPs correlates with the higher toxic effects on microorganisms, which have relatively large interfacial area thereby increasing their antibacterial effectiveness.[34] In our previous reports, the size distribution (DLS) of the AgNPs,[27] CuONPs,[28] and Ag-CuO NCs[29] was discussed. The broad XRD peaks clearly indicated the purity of the green fabricated AgNPs, CuONPs, and Ag-CuO NCs. The diffraction peaks were observed at 27.89°, 32.29°, 38.2°, 44.4°, and 46.29°. The crystallographic planes corresponded to (1 1 0), (1 0 0), (0 0 2), (2 0 0), and (2 0 2) represent the FCC monoclinic crystal structure of Ag-CuO NCs. The green synthesized AgNPs (JCPDS card no: 01-1013) and CuONPs (JCPDS card no: 80-1916) composition were attributed to Ag-CuO NCs confirmed by XRD analysis. HR-TEM analysis of green synthesized AgNPs showed spherical in shape,[27] CuONPs showed in spherical and rod shape,[28] and the Ag-CuO NCs showed intercalate to AgNPs and CuONPs, as spherical and rod-shaped structure.[29]

The fluorescence studies were carried out for the prepared NPs; thus, AgNPs, CuONPs, and Ag-CuO NCs are apparently having good optical as well as biological properties. Besides, the NPs as prepared are generally based on photonic nanomaterials as well.[35] Hence, the fluorescence spectrum was recorded by fluoromax spectrofluorometer at an excitation source of 150 W ozone-free xenon arc lamp. The excitation ranges were 270, 300, and 280 nm for the AgNPs, CuONPs, and Ag-CuO NCs respectively. The collected emission (or) recombination peaks were 375–440 nm, 405–445 nm, and 385–445 nm for the AgNPs, CuONPs, and Ag-CuO NCs respectively. Fluorescence emission spectra of green synthesized AgNPs, CuONPs, and Ag-CuO NCs showed distinct peaks recorded at 393 nm, 412 and 436 nm, and 394, 410, and 435 nm, respectively. The AgNPs showed peak from 375 nm to gradually increased intensity up to 393 nm; then the band slowly decreased to 440 nm (Figure 1a). Similar result has been reported in bio-inspired AgNPs using leaf extract of *Pedalium murex*, the broad emission peak observed at 478 nm after which was slowly decreased up to 650 nm and the emission spectra $\lambda_{ex} = 430$ nm.[36] The CuONPs observed sharp fluorescence emission peak at 412 and 436 nm, whereas the CuONPs' peak range starts from 405 to slowly increased peak up to 412 and 436 nm to represent the synthesized CuONPs (Figure 1b). The broad band of CuONPs showed violet-blue luminescent shoulder peak obtained at 412 nm, which has been near-band-edge emission peak of CuO. Further, the CuONPs showed 436 nm peak, which was the existence of Cu in CuO and denoted as p-type semiconductor. The present results are correlated with previous reports.[37] The CuO nanobelts exhibit direct band gap energy value is 3.2 eV, which can be attributed to larger value than the bulk CuO and relatively quantum size effects.[38] Green synthesized hybrid Ag-CuO NCs showed three prominent peaks well associated with AgNPs and CuONPs, which showed significant emission spectra of Ag-CuO NCs (Figure 1c). Yang et al.[39] stated that the Ag-CuO nanocomposite comparatively lower than the CuO nanosheet emission intensity, as well as the Ag NPs, creating the separation of photo-induced electrons and holes that enhance the photocatalytic performance. Silver/cobalt nanoparticles (Ag/Co NPs)

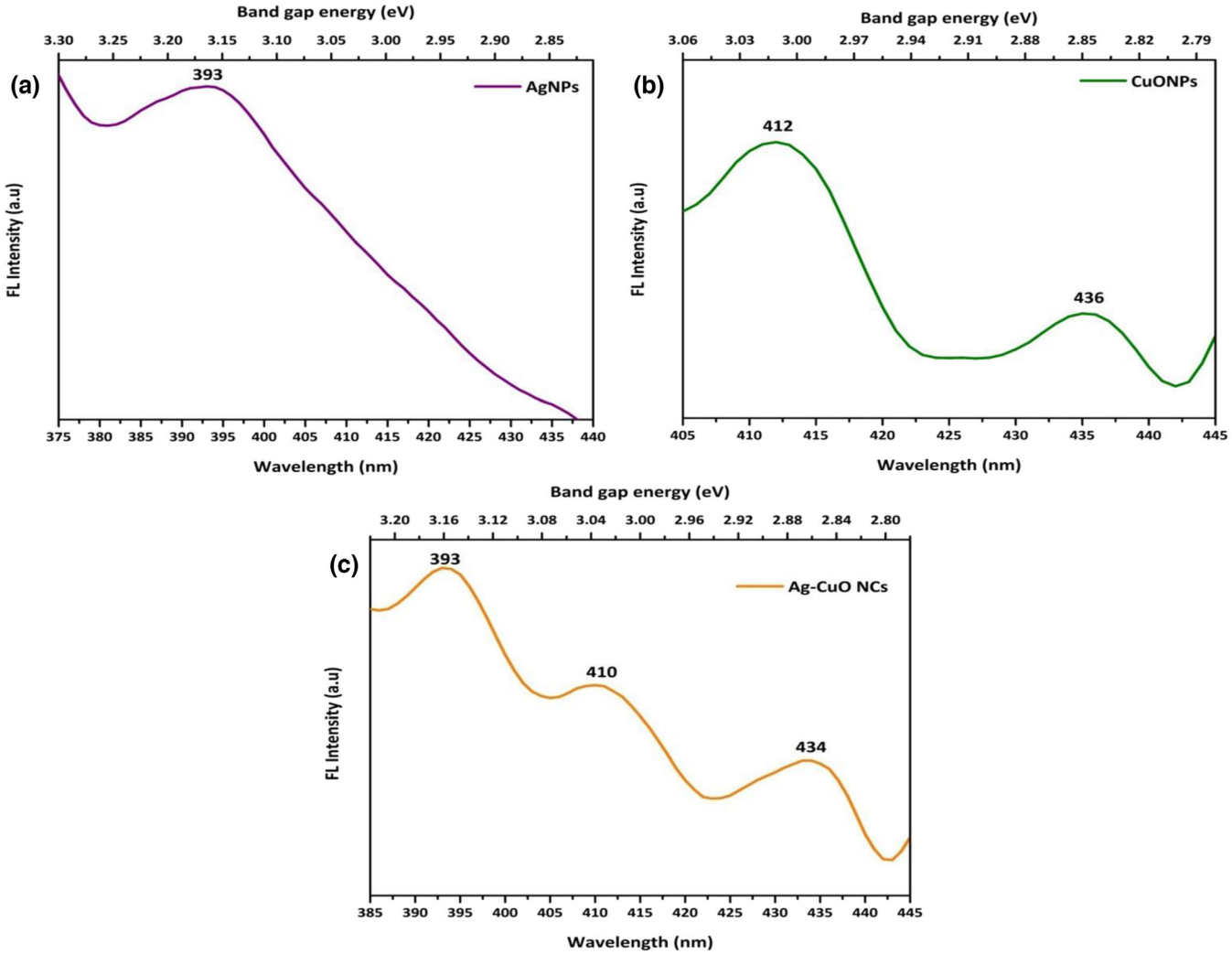


**FIGURE 1** Fluorescence emission spectra of green synthesized AgNPs (a), CuONPs (b), and Ag-CuO NCs (c).

showed excitation wavelength below 420 nm; therefore, the shorter peak cannot be seen. When the excitation wavelength range increases, the later peak become red shifted and distinct.

### 3.1.1 | Raman spectroscopy analysis

Raman spectroscopy is a rapid and sensitive surface detection technique used to identify the chemical interactions of metal NPs and susceptible interfacial studies with significant advantages.[40] Green fabricated AgNPs exhibited four distinct peaks at 474.66, 1249.7, 1664.31, and 1827.47 $cm^{-1}$; CuONPs showed peaks at 132.06, 305.98, 799.58, and 906.71 $cm^{-1}$; and Ag-CuO NCs revealed peaks at 368.05, 675.22, 1354.11, 1605.17, 2325.47, and 2918.09 $cm^{-1}$. The strong signals of green synthesized AgNPs (Figure 2a), CuONPs (Figure 2b), and Ag-CuO NCs (Figure 2c) were clearly indicated by the Raman spectroscopy analysis. The green synthesized AgNPs showed sharp peaks at 474.66 $cm^{-1}$ stretching vibration of C–N–C and C–S–C, 1249.7 and 1664.31 $cm^{-1}$ carboxylic symmetric and antisymmetric C=O stretching vibration of carboxylic group. The AgNPs' 474.66, 1249.7, and 1664.31 $cm^{-1}$ peaks are closely correlated to previous report of 572.6, 1350.0, and 1587.0 $cm^{-1}$.[41] The CuONPs peaks at 132.06 $cm^{-1}$ corresponding to the phase rotation (Ag) mode, 305.98 and 799.58 $cm^{-1}$ symmetrical stretching of oxygen (Bg) mode, 906.71 $cm^{-1}$ in accordance with the C=O symmetrical and asymmetrical stretching vibration of carboxylic group. The characteristic bands of CuONPs were 305.98, 799.58, and 906.71 $cm^{-1}$; these corresponding peaks well match with 294, 478, and 581 $cm^{-1}$.[42] Raman spectra of Ag-CuO NCs exhibited that AgNPs and CuONPs peaks are correlated to these bands at 368.05, 675.22, 1354.11, 1605.17, 2325.47, and 2918.09 $cm^{-1}$. Sridevi et al.[43] reported that the ternary nanocomposites fabricated by hydrothermal method of reduced graphene oxide /copper oxide/silver (rGO/CuO/Ag NCs) were attributed to 1336, 1576, and 2673 $cm^{-1}$.

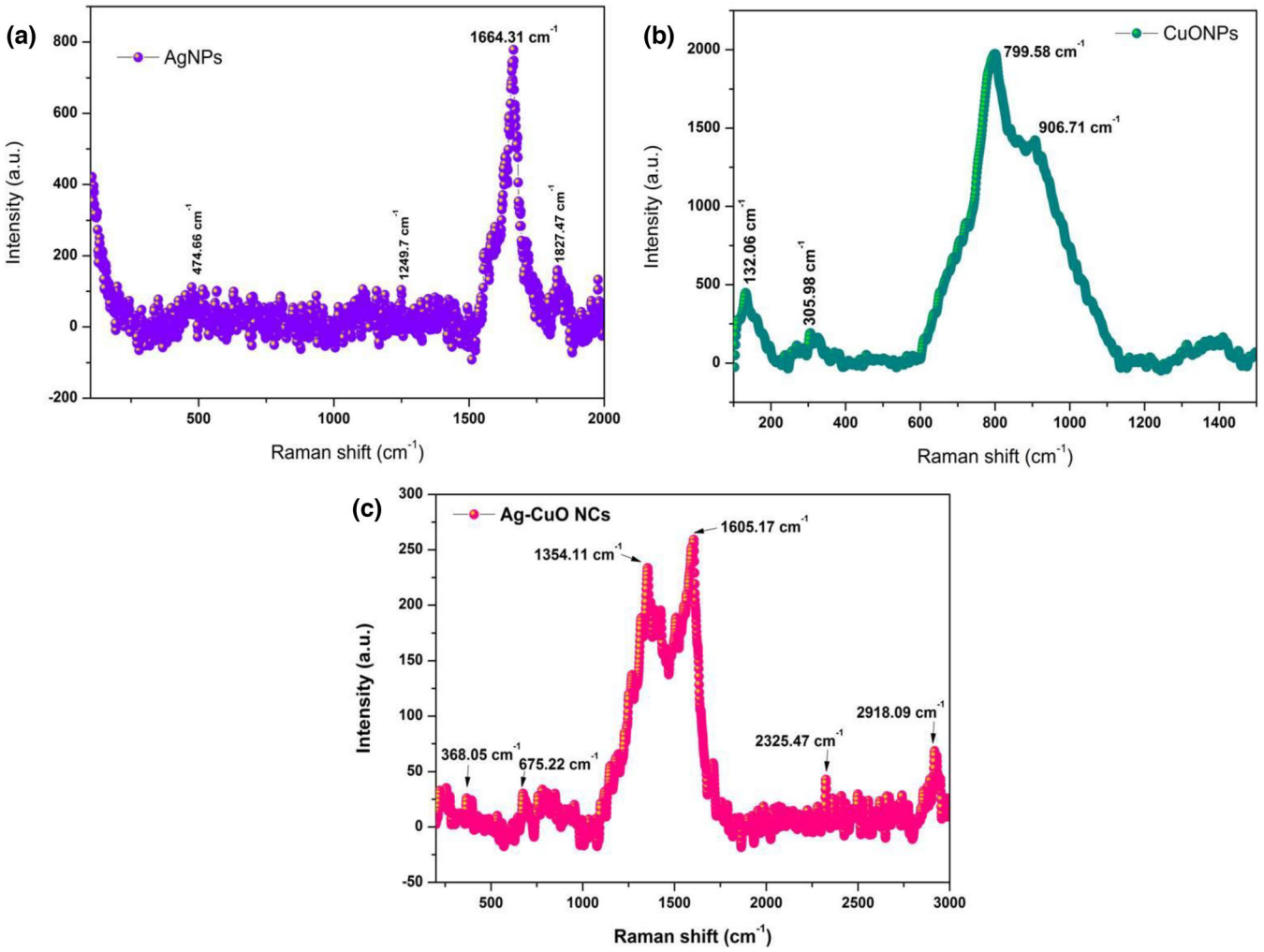


**FIGURE 2** Raman spectral analysis of green synthesized AgNPs (a), CuONPs (b), and Ag-CuO NCs (c).

The 1336 and 2673 $cm^{-1}$ bands were assigned to κ-point phonons of A1g symmetry and the stretching of C $sp^2$ pair atoms, respectively.

### 3.1.2 | FE-SEM elemental mapping with EDX analysis

The microstructure of the green synthesized AgNPs, CuONPs (Figure S2), and Ag-CuO NCs (Figure S3) was visualized under FE-SEM. The surface topology and elemental composition of the nanomaterials were analyzed through EDX technique. The microstructure of the green synthesized AgNPs showed spherical shape (Figure 3a), and the particles are in nonuniform distribution (Figure S1). Major signals of AgNPs represent the Ag and Au as secondary peak from surface coating material (Figure 3b,c). The EDX analysis of AgNPs clearly indicated high purity index of Ag (96.90%) and Au (3.10%) as a secondary peak from surface gold sputtering during sample preparation (Figure 3d). Similar results recently reported that the AgNPs synthesized using *Pseudomonas putida* and *Escherichia coli* showed silver signals from both organisms. The EDX technique was used to determine the elemental composition and other impurities.[44] The green synthesized CuONPs showed spherical and hexagonal like shape (Figure 4a) with non-uniform distribution (Figure S2). Elemental mapping of CuONPs displayed strong signals for copper (Cu), oxygen (O), and gold (Au) (Figure 4b,c). EDX analysis of CuONPs revealed that the Cu (66.88%), O (30.77%), and Au (2.34%) strongly represent high purity of green synthesized CuONPs (Figure 4d). Nagajyothi et al.[45] stated that the CuONPs from aqueous extract of black bean showed uneven shape of spherical and hexagonal structure. Elemental mapping also revealed the Cu and O signals. Green synthesized Ag-CuO NCs appeared as smaller spherical and hexagonal shape (Figure 5a). Figure S3 clearly indicates the successful formation of Ag-CuO NCs due to the incorporation of AgNPs and CuONPs.

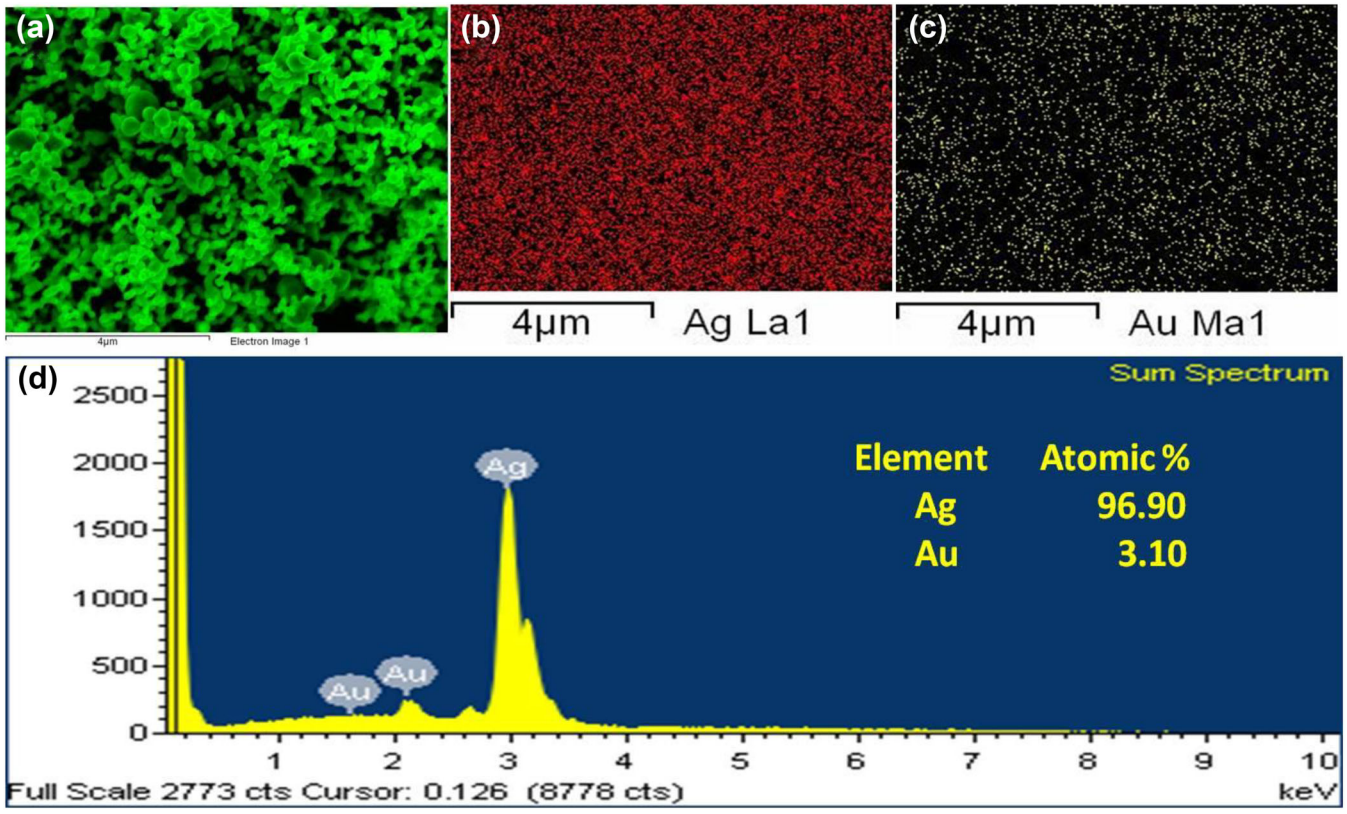


**FIGURE 3** Elemental mapping and EDX spectrum analysis of green synthesized AgNPs. Electron image of AgNPs (a), Ag (b), Au (c), and EDX (d).

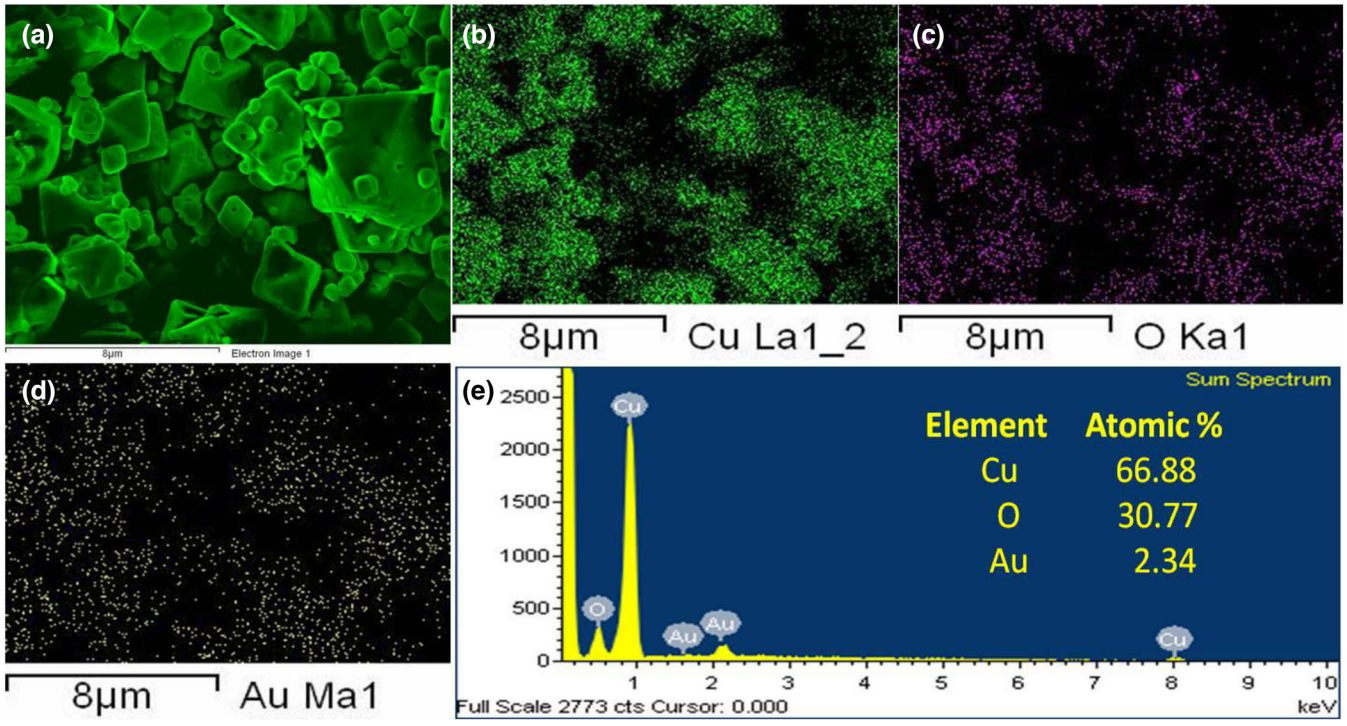


**FIGURE 4** Elemental mapping and EDX spectrum analysis of green synthesized CuONPs. Electron image of CuONPs (a), Cu (b), O (c), Au (d), and EDX (e).

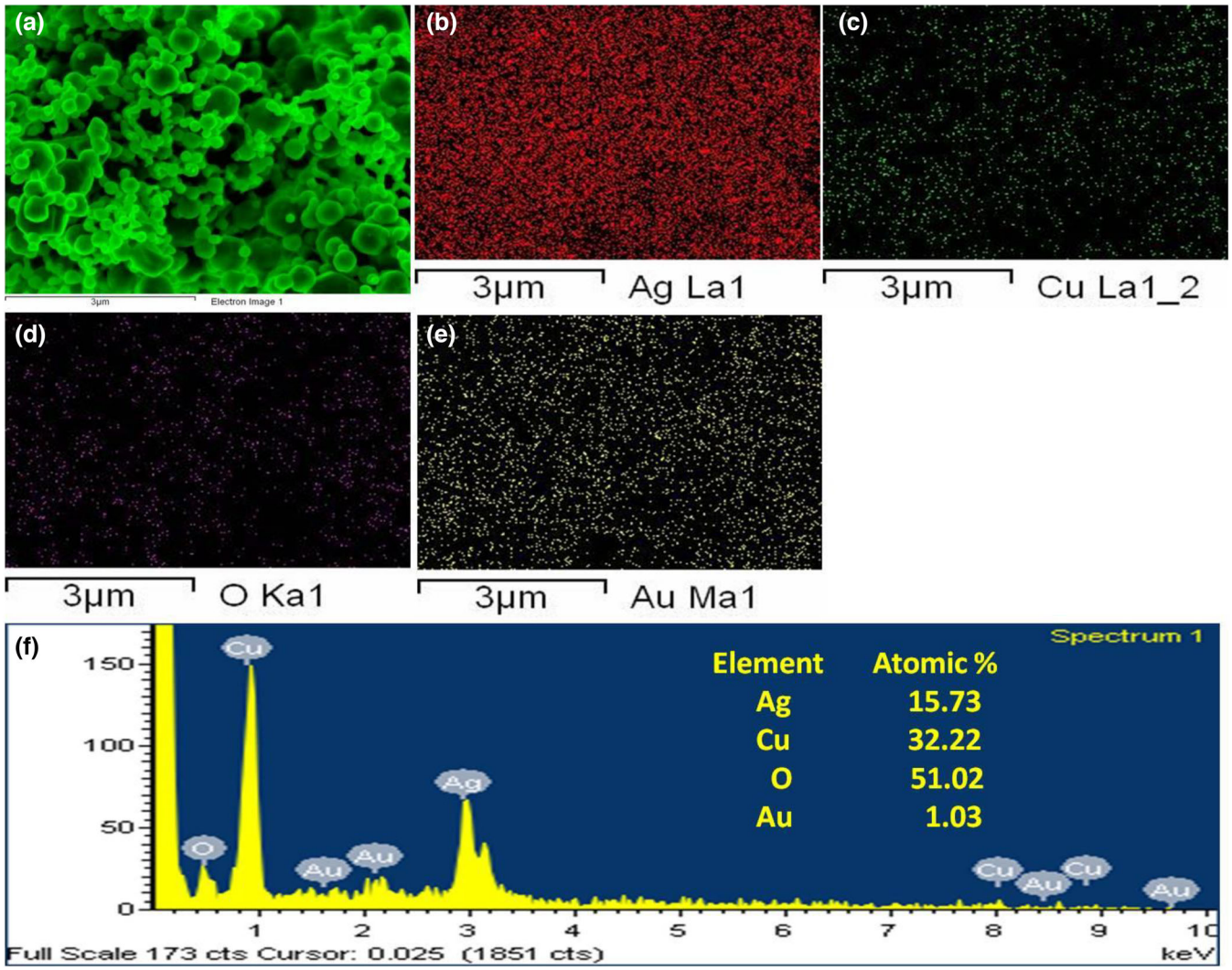


FIGURE 5 Elemental mapping and EDX spectrum analysis of green synthesized Ag-CuO NCs. Electron image of Ag-CuO NCs (a), Ag (b), Cu (c), O (d), Au (e), and EDX (f).

Elemental mapping of Ag-CuO NCs showed Ag, Cu, and O strong signals, which clearly indicate the successful distribution and incorporation of the elements (Figure 5b–e). Further, it was analyzed by EDX spectrum, which showed major peaks for Ag (15.73%), Cu (32.22%), O (51.02%), and Au (1.03%) and strongly suggested the high purity of green synthesized Ag-CuO NCs (Figure 5f). The FE-SEM analysis of ternary CuO decorated $Ag_3AsO_4$/GO exhibits signals (Ag, As, O, C, and Cu) detected from element mapping; further, it was confirmed by the EDX analysis to validate the elements.[46]

### 3.1.3 | Thermal behavior of nanomaterials

The thermal behavior of green synthesized AgNPs, CuONPs, and Ag-CuO NCs were analyzed by thermogravimetric (TGA) and differential scanning calorimetry (DSC) under high temperature. The thermal stability and purity of the AgNPs showed weight loss before the temperature 100°C, due to the moisture from biomolecules that capped the surface of the NPs.[47] TG analysis of AgNPs, CuONPs, and Ag-CuO NCs and their total weight loss obtained were 0.8% (Figure 6a), 8.5% (Figure 6b), and 3.17% (Figure 6c), respectively. No significant loss of weight observed at 200°C by the AgNPs, CuONPs, and Ag-CuO NCs (Figure 6a–c). The temperature-dependent weight loss of AgNPs were 0.064% in 200°C, 0.592% in 380°C, 0.095% in 460°C, and 0.05% in 700°C. The CuONPs' weight loss showed 0.176% in 100°C, 10.275% in 300°C, −1.39% in 500°C, and −0.496% in 700°C. The Ag-CuO NCs showed weight loss of 0.01% in 150°C, 4.182% in 350°C, −0.293% in 450°C, and −0.722% in 700°C. In contrary, the negative impact of weight loss happened in the CuONPs and Ag-CuO NCs. When compared with CuONPs and Ag-CuO NCs, the AgNPs were

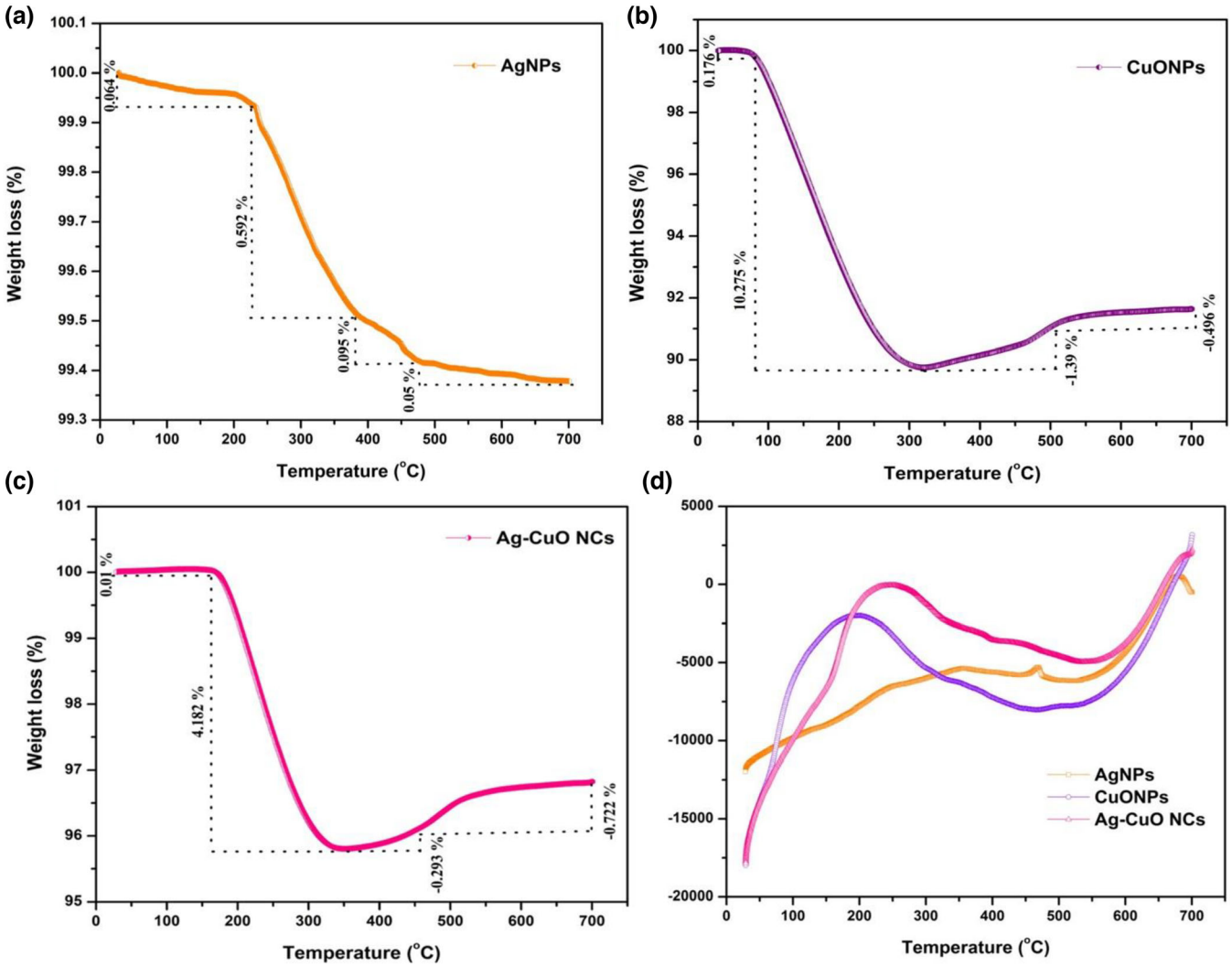


**FIGURE 6** TG analysis of green synthesized AgNPs (a), CuONPs (b), Ag-CuO NCs (c), and DSC analysis of AgNPs, CuONPs, and Ag-CuO NCs (d).

thermally stable with 0.8% weight loss. Due to the breakdown of plant-derived phytochemicals such as carbohydrates, flavonoids, and phenolic acids, which served as stabilizing agents for the formation of AgNPs, this also caused weight loss in AgNPs. Temperature reached 440°C, and the weight of the AgNPs decreased by about 3.46%, due to the resistant phytochemicals capped on the surface of the NPs.[48] From the TGA results, it strongly indicated that the *O. americanum* L. aqueous leaf extract embedding on surface of the AgNPs, CuONPs, and Ag-CuO NCs. From the DSC analysis of AgNPs, CuONPs, and Ag-CuO NCs revealed endothermic and exothermic curves depicted in Figure 6d. The exothermic peaks of AgNPs (240°C, 357.81°C, 464.26°C), CuONPs (184.29°C, 296.76°C, 500.22°C), and Ag-CuO NCs (241.44°C, 384.74°C, 435.56°C) correspondence with desorption of phytochemical constituents anchored to the AgNPs' surface.[49]

## 3.2 | Effect of AgNPs on growth rate of pathogenic microorganism

The growth rate dynamics of pathogenic Gram-negative bacteria *A. hydrophila*, *P.* aeruginosa, and Gram-positive bacteria *S. aureus* with the presence of green synthesized AgNPs exhibited that the AgNPs displayed dose-dependent inhibitory activity (10–100 μg/mL) against the tested bacteria. Figure 7 showed green synthesized AgNPs potent growth inhibitory activity against *A. hydrophila* (Figure 7a) and *S. aureus* (Figure 7c), when compared with *P. aeruginosa* (Figure 7b). Shrivastava et al.[50] stated that the green synthesized AgNPs were potent inhibitory agent against Gram-negative bacteria comparing to the Gram-positive bacteria. Due to the presence of thick peptidoglycan later in Gram-positive bacteria, the penetration ability of AgNPs was restricted. AgNPs can directly bind to the cell surface of a wide variety of

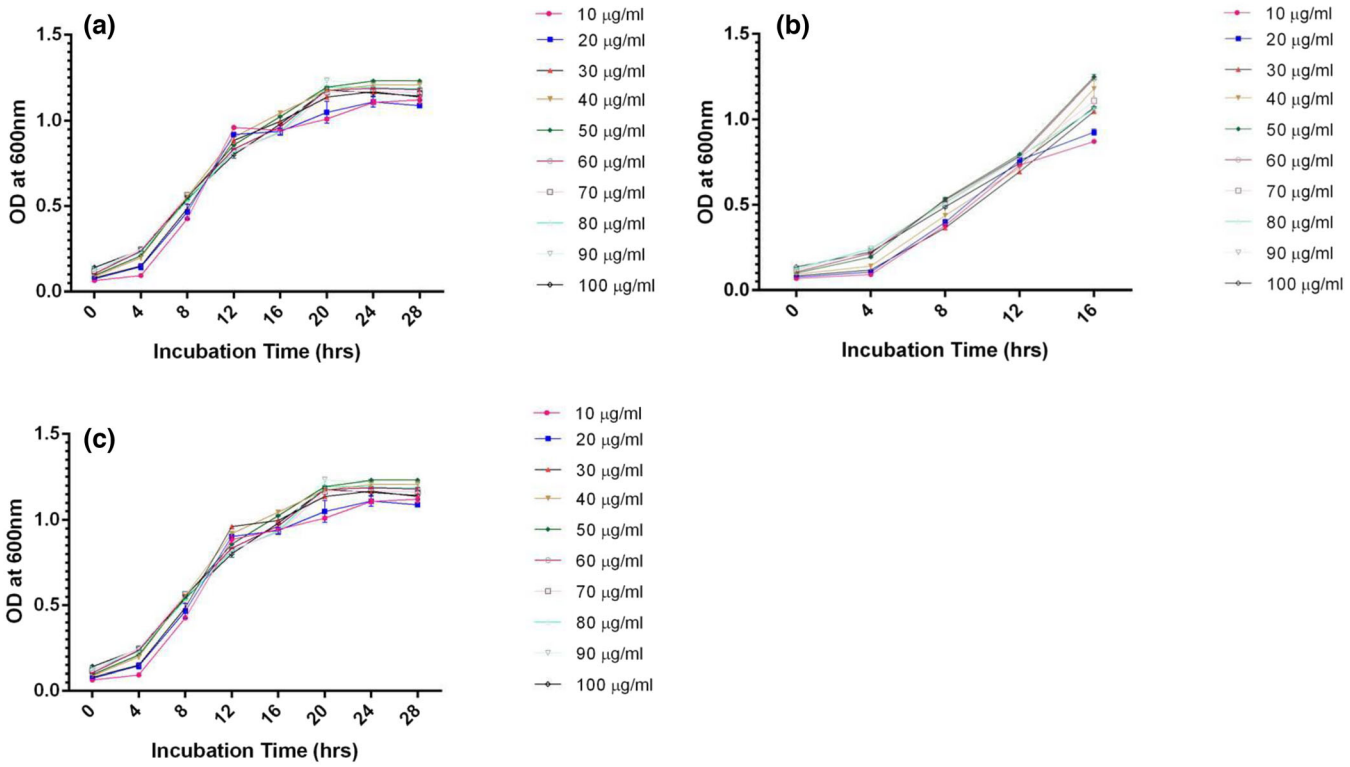


**FIGURE 7** Growth rate analysis of green synthesized AgNPs treated against *Aeromonas hydrophila* (a), *Pseudomonas aeruginosa* (b), and *Staphylococcus aureus* (c).

bacteria.[51] Gram-negative bacteria are more competitive than Gram-positive bacteria because they can readily adjust their pathogenicity through mechanisms involve in reducing virulence or either proliferation of the microorganisms. AgNPs are an outstanding performer against various bacterial cells, and their growth has been effectively inhibited.[52] They have special account on clinical therapeutics because of their acceptable toxic effect on mammalian cells and they promote infectious chronic wound healing.[53] The antibacterial action of size-tunable AgNPs has been significantly influenced; smaller NPs exhibit stronger bioreactivity than bigger ones. Improved antibacterial activity is directly correlated with smaller AgNPs. In addition to the two different modes of action, contact angle and $Ag^+$ release,[34] our previous study reported that the higher bacterial growth reduction was obtained for green synthesized AgNPs, due to the higher surface area to volume ratio, easy penetration of cellular membrane, and the cationic AgNPs dissolved in water or enter cells, and small amount of silver (Ag) is released.[27] In consequences, NPs have bactericidal effect than free Ag ions, with the antibacterial effects contributed by the physicochemical parameters of the nanoparticles and silver ion elution.[54] AgNPs synthesized using kaolin and *Ficus carica* on chitosan food packaging film (Cht/KC/AgNPs) were evaluated against pathogenic microorganisms *E. coli* and *S. aureus* and attributed decreased development of bacterial growth, and AgNPs could be used for food preservation.[55]

### 3.2.1 | Effect of CuONPs on growth rate of pathogenic microorganism

Effect of green fabricated CuONPs treated against Gram-negative and Gram-positive bacteria with dose-dependent (10–100 µg/mL) inhibitory activity was showed in Figure 8. The CuONPs showed decreased bacterial growth rate pattern of pathogenic microorganisms (Figure 8a–c). When compared to CuONPs, the AgNPs had potential antibacterial activity against pathogens. The copper nanoparticles (CuNPs) have been used to inhibit the bacterial growth, which can be attributed to higher electron transfer into bacteria. Furthermore, copper's antibacterial properties are effective in cellular damaging due to the contact between released $Cu^{2+}$ ions and bacterial membranes. On the other hand, CuNPs are more unstable and prone to oxidation. This issue was solved by converting CuNPs to CuONPs, which have higher stability but slightly lower activity.[56] The antibacterial activity of CuONPs has not been well understood, but it is assumed to involve in bacterial cell wall adhesion

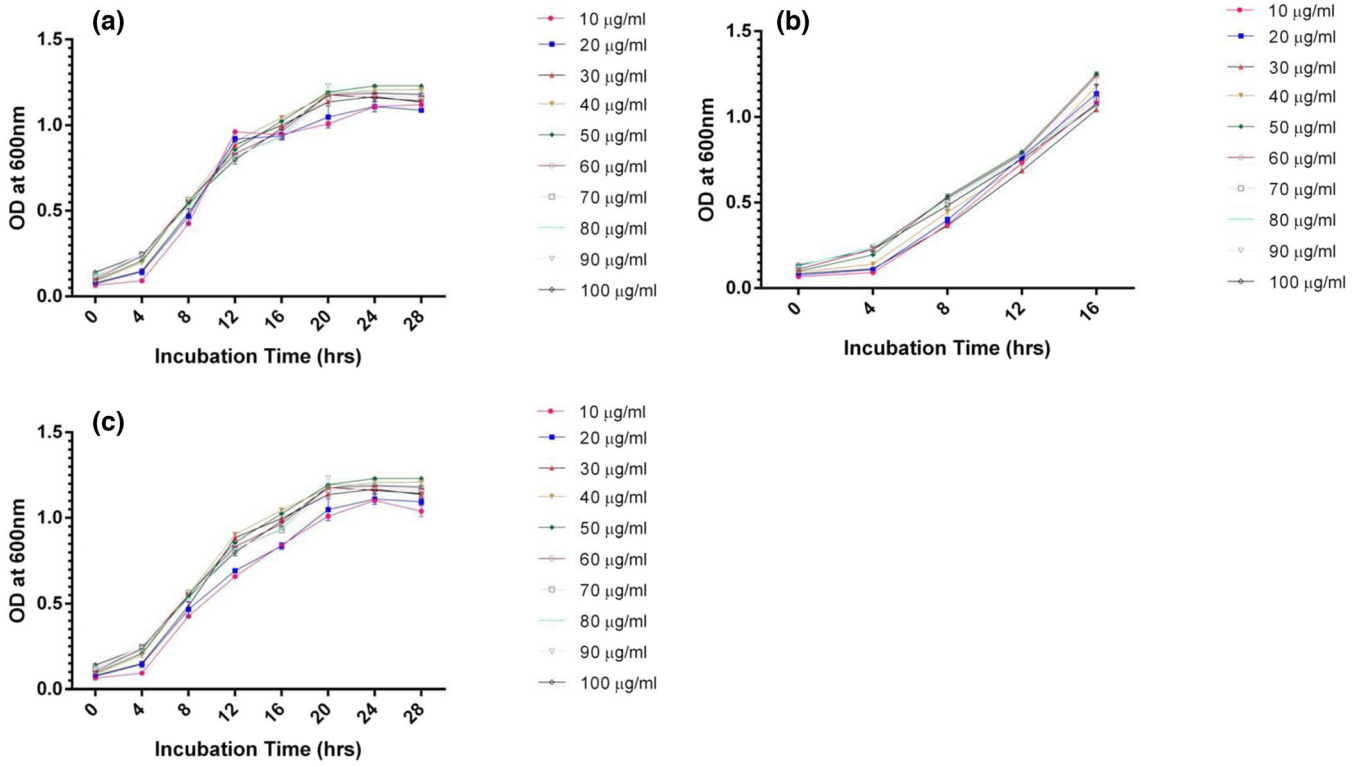


**FIGURE 8** Growth rate analysis of green synthesized CuONPs treated against *Aeromonas hydrophila* (a), *Pseudomonas aeruginosa* (b), and *Staphylococcus aureus* (c).

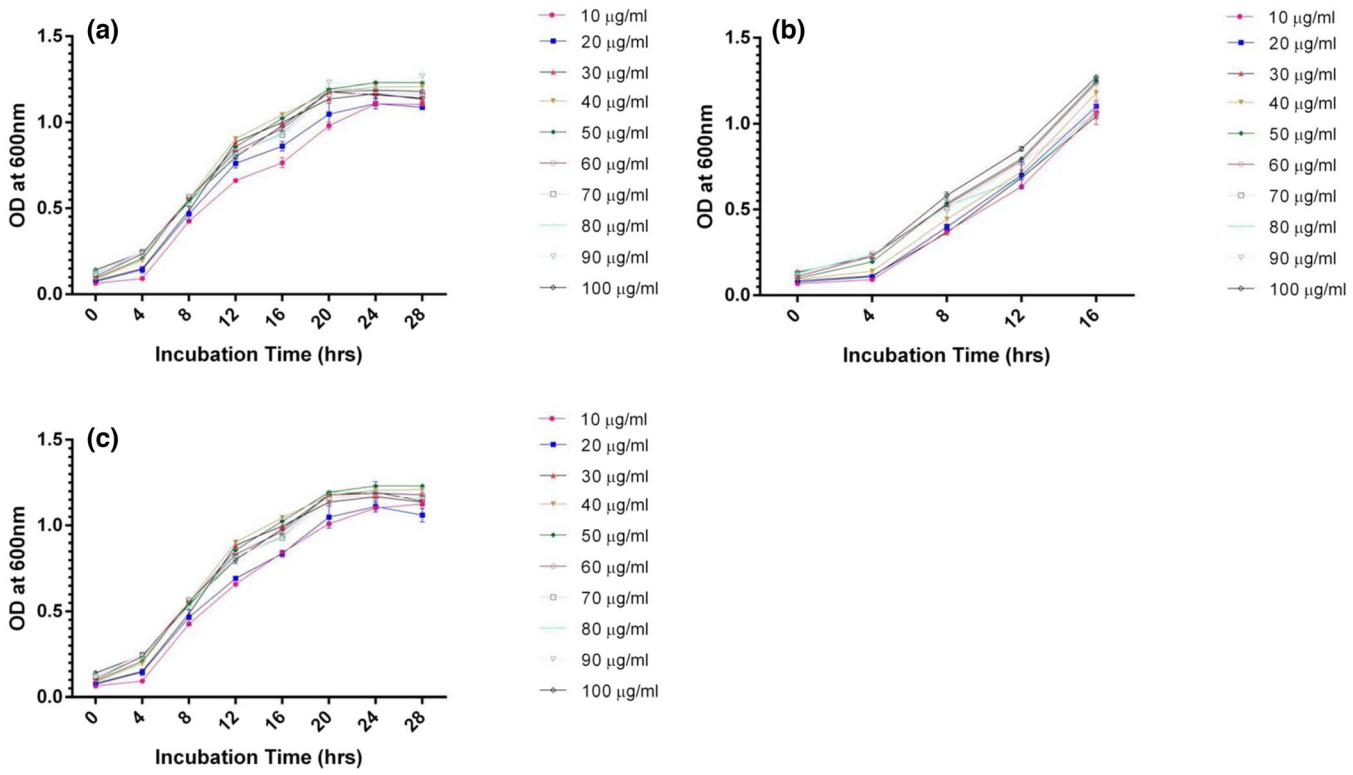


**FIGURE 9** Growth rate analysis of green fabricated hybrid Ag-CuO NCs treated against *Aeromonas hydrophila* (a), *Pseudomonas aeruginosa* (b), and *Staphylococcus aureus* (c).

stimulated by electrostatic interactions.[57] Dissociation of $Cu^{2+}$ can induce the production of reactive oxygen species (ROS) that could damage the cellular membranes. These ions may possess the ability to penetrate the cell, causing membrane destruction and releasing the internal content of the cell that leads to bacterial cell leakage.[58]

### 3.2.2 | Effect of Ag-CuO NCs on growth rate of pathogenic microorganism

The green fabricated hybrid Ag-CuO NCs were tested against pathogenic Gram-positive and Gram-negative bacterial growth kinetics. The dose-dependent inhibitory activity was measured at varying concentrations of Ag-CuO NCs (10–100 μg/mL) (Figure 9). One substantial limitation of this technique is the difficulty in determining the amount of antibacterial activity with subject to time.[59] The green fabricated hybrid Ag-CuO NCs had potential growth inhibition on both Gram-negative and Gram-positive bacteria. Growth kinetics of hybrid Ag-CuO NCs decreased the bacteria population from 0 to 4 h, and after 4 h, both Gram-positive and Gram-negative bacteria overcome the NCs activity and increased their population (Figure 9a–c). Figure 9b showed growth kinetics of *P. aeruginosa*, and Ag-CuO NCs inhibited the growth till 4 h. The decline phase of bacterial growth rate was observed in *A. hydrophila* and *P. aeruginosa* after 20 h. During the death phase of bacterial growth rate analysis, viable cells geometrically decreases. Asamoah et al.[60] reported that the comparative analysis of CuO/Ag and ZnO/Ag nanocomposites exhibited broad spectrum of antibacterial activity against pathogenic microorganisms such as *E. coli* and *S. aureus*. The NCs incorporate the toxic effects of diverse elemental compositions to produce an antibacterial synergy. Bacterial cells are sensitive to various transition metals. The NCs combine various transition metals and display broad-spectrum bacteria susceptibility.[61] AgNPs decorated CA/PUF-Ag composites have potent antibacterial efficacy compared with pure polyurethane (PUF) and calcium alginate (CA)/PUF. AgNPs release $Ag^{+}$ ions that interact with ATP production, DNA replication, and increase ROS generation, which interfere with internal substances and destroy the cell membrane of *E. coli*.[62] The fabrication of NCs using metal oxide NPs provide a low-cost, high-efficient antibacterial agent. The antimicrobial activity of polyacrylic acid (PAA) regulated silver carried copper oxide (CuO@Ag) nanosheet composites tested against pathogenic microorganisms, especially the synthesized CuO@Ag demonstrated excellent antibacterial activity against *S. aureus*. The CuO@Ag nanosheet composites exhibit destruction of bacterial cell membrane and the subsequent leakage of the cytoplasm caused by the release of $Ag^{+}$ and $Cu^{2+}$.[63]

## 3.3 | Evaluation of antibiofilm activity

Biofilm are bunch of microbial communities, which can be linked together to secrete polymers and growing on any type of surfaces, either living or nonliving.[64] The AgNPs have strong antibacterial activity against Gram-positive and Gram-negative pathogens.[65] CuONPs are widely available, economical, stable, less toxic to the mammalian cells, and environmental friendly. Both the materials have individual unique physicochemical properties, and the combinatorial effect in the form of Ag-CuO NCs is prominent to biological activities compared to the individual NPs.[66] In the present study, green fabricated AgNPs, CuONPs, and Ag-CuO NCs were tested against aquaculture important pathogenic Gram-negative and Gram-positive bacteria such as *A. hydrophila*, *P. aeruginosa*, and *S. aureus*. These opportunistic pathogens cause various diseases to the aquatic animals as well as human.[67]

Microorganisms can form biofilm with diversified exopolysaccharide (EPS) production in bacteria involved through three pathways such as Wzx/Wzy-dependent, synthase-dependent, and ABC transporter-dependent pathway.[68] The dose-dependent antibiofilm activity of AgNPs, CuONPs, and Ag-CuO NCs was shown in Figure 10. These materials are compared with the positive control, and the results showed potent biofilm inhibitory responses against *A. hydrophila*, *P. aeruginosa*, and *S. aureus*. No antibiofilm inhibitory activity was observed in negative control. The AgNPs showed antibiofilm activity against *A. hydrophila* (69%), *P. aeruginosa* (71.37%), and *S. aureus* (66.96%) at 100 μg/mL (Figure 10a). Similar levels of biofilm inhibition were observed for AgNPs irrespective of organisms. Green synthesized CuONPs showed antibiofilm activity against *P. aeruginosa* (64.89%), *A. hydrophila* (60.22%), and *S. aureus* (49.30%) (Figure 10b). The Ag-CuO NCs showed potential antibiofilm activity in *A. hydrophila* (74.24%), *P. aeruginosa* (65.44%), and *S. aureus* (72%) (Figure 10c).

Earlier studies stated that CuONPs tested on biofilm activity of methicillin-resistant *Staphylococcus aureus* (MRSA) and *E. coli* demonstrated increased biofilm inhibition based upon dose-dependent concentration of nanoparticles.[69] AgNPs have also been showed to inhibit *P. aeruginosa* biofilms approximately four- to sixfold,[70] whereas Zn/CuO NCs and CuONPs inhibited *Streptococcus mutans* biofilms approximately 88% and 70%, respectively.[71] Jang et al.[72] stated that the synthesized bimetallic Ag/Cu nanoparticles on a graphene oxide

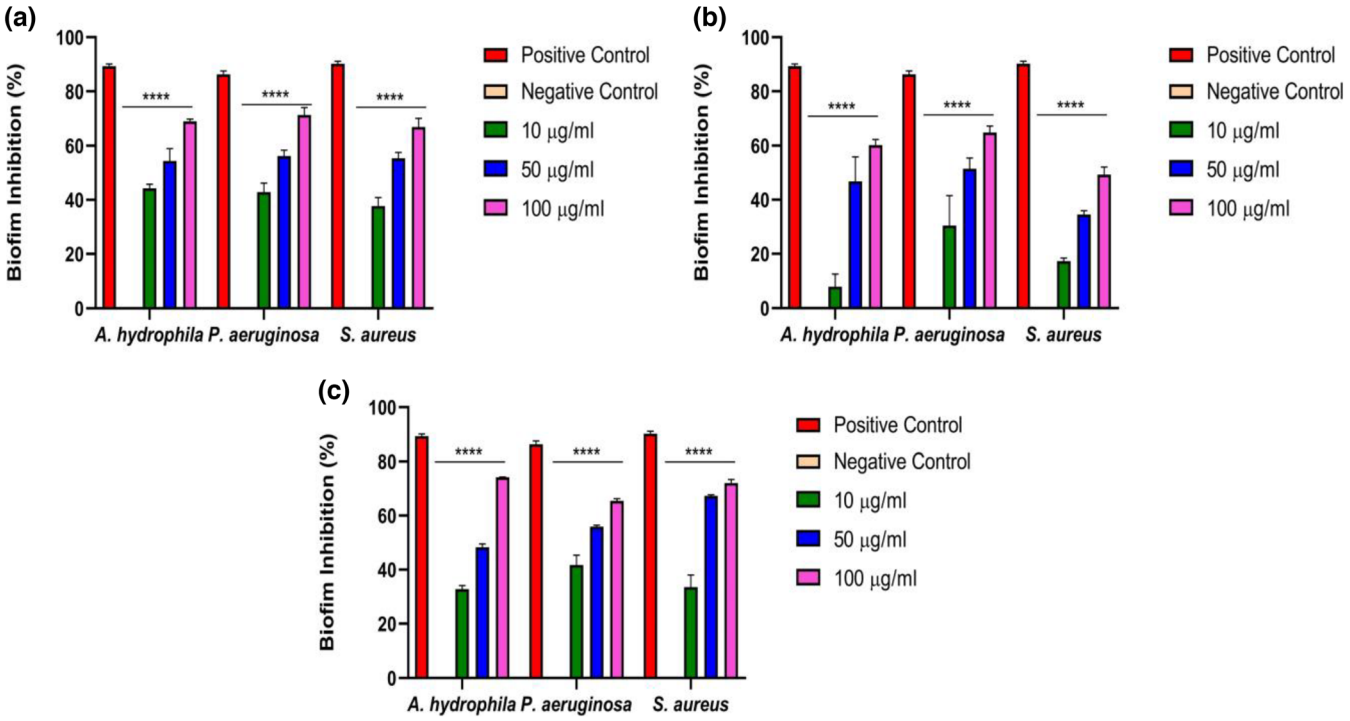


**FIGURE 10** Anti-biofilm inhibition activity of green fabricated AgNPs (a), CuONPs (b), and Ag-CuO NCs (c) treated against *Aeromonas hydrophila*, *Pseudomonas aeruginosa*, and *Staphylococcus aureus*. *, **, ***, and **** indicate significant difference of P-values are ≤0.05, ≤0.01, ≤0.001, and ≤0.0001, respectively.

(GO) surface (Ag/Cu/GO) could prominently inhibit the biofilm formation of antibiotic resistant bacteria. The present study showed maximum biofilm inhibition on *A. hydrophila* (74.24%) and *S. aureus* (72%) at 100 µg/mL concentration of green fabricated Ag-CuO NCs.

## 3.4 | Confocal laser scanning microscopic analysis

The morphological variations in the biofilm architecture, surface area colonization, and thickness were observed under the CLSM. The formation of distinct biofilm architecture is the most important step in biofilm development.[73] CLSM images demonstrated changes in the biofilm thickness as well as biofilm structural morphology modifications. The two-dimensional (2D), three-dimensional (3D), and intensity images confirmed the reduction in size and thickness of *A. hydrophila* (Figure 11), *P. aeruginosa* (Figure 12), and *S. aureus* (Figure 13) biofilm treated with AgNPs, CuONPs, and Ag-CuO NCs. Based on the AO/EB staining, the green color fluorescence emitted by live cells, whereas the red color fluorescence exhibited by dead cells. The obtained red color is due to presence of dead cells caused by increased concentration of nanomaterials through membrane damages. The release of EPS from the surface of the bacterial cell wall continues to be a significant factor in the adhesive habitat of bacteria and the development of thick bacterial biofilms, might be the intellect of a reduction in bacterial biofilm matrix thickness.[74]

Mature biofilms are difficult to eradicate due to their susceptibility to host defense mechanisms and antimicrobials. Antibiotic resistance was substantially improved by phenotypic changes found in mature *P. aeruginosa* biofilms.[34] As a result, eliminating biofilms in their early stages are faster and more beneficial. The present study found that Ag-CuO NCs effectively inhibited the biofilm growth of *A. hydrophila* (Figure 11), *P. aeruginosa* (Figure 12), and *S. aureus* (Figure 13) by decreasing the biofilm surface area coverage. Compared to the negative control, the treatment of positive control (streptomycin) followed with respective green synthesized AgNPs, CuONPs, and Ag-CuO NCs showed the significantly reduced biofilm formation and micro-colony formation in *A. hydrophila*, *P. aeruginosa*, and *S. aureus*. This perspective on Ag-CuO NCs gets it closer to being an ideal quorum sensing inhibitor.

AgNPs are capable of inhibiting the growth and reduce the microbial population through a variety of mechanistic ways. Currently, AgNPs are recognized as an antimicrobial agent.[75] In brief, $Ag^{+}$ ions communicate

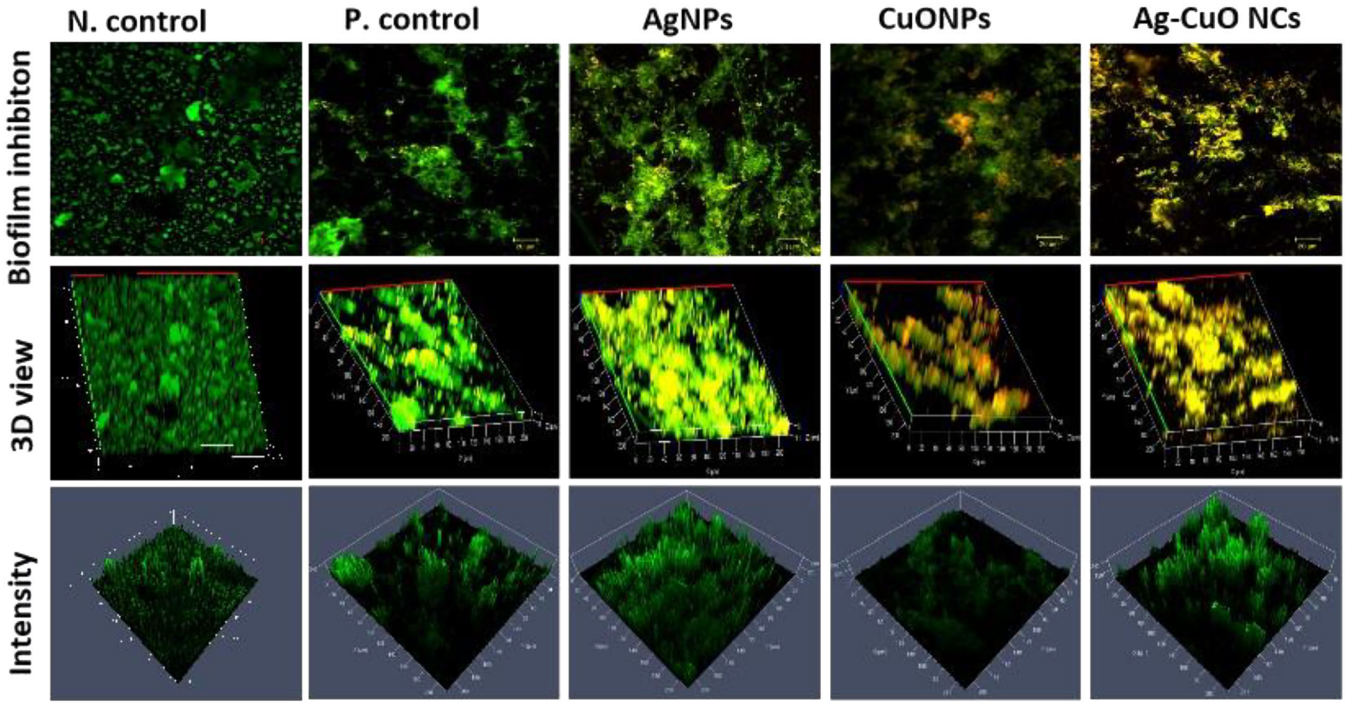


**FIGURE 11** Confocal laser scanning microscope (CLSM) image of *Aeromonas hydrophila* biofilm formation treated with green fabricated AgNPs, CuONPs, and Ag-CuO NCs (100 μg/mL). Panel of images show the three-dimensional view of biofilm formed by control and treated cultures and their two-dimensional views with their respective intensity projections. Each experiment was performed using three independent cultures, and one representative data set is shown here. Scale bars = 50 μm.

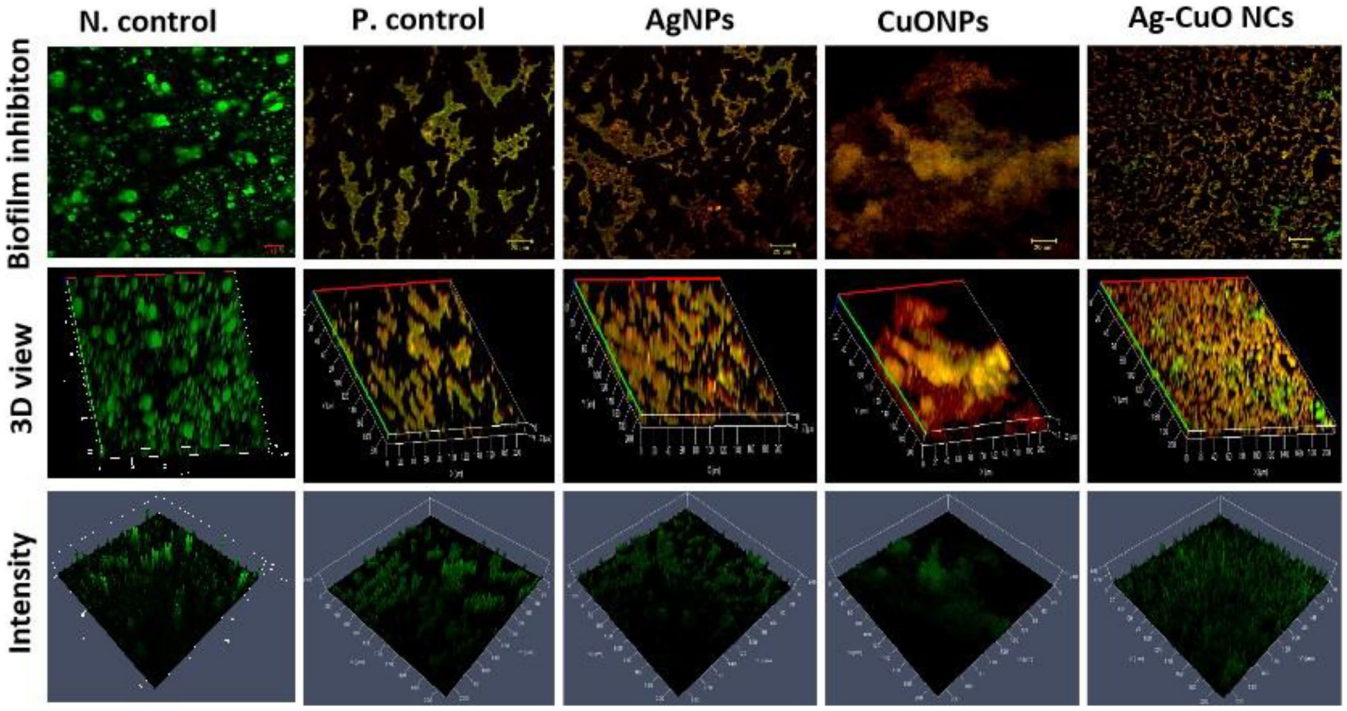


**FIGURE 12** CLSM image of *Pseudomonas aeruginosa* biofilm formation treated with green fabricated AgNPs, CuONPs, and Ag-CuO NCs (100 μg/mL). Panel of images show the three-dimensional view of biofilm formed by control and treated cultures and their two-dimensional views with their respective intensity projections. Each experiment was performed using three independent cultures, and one representative data set is shown here. Scale bars = 50 μm.

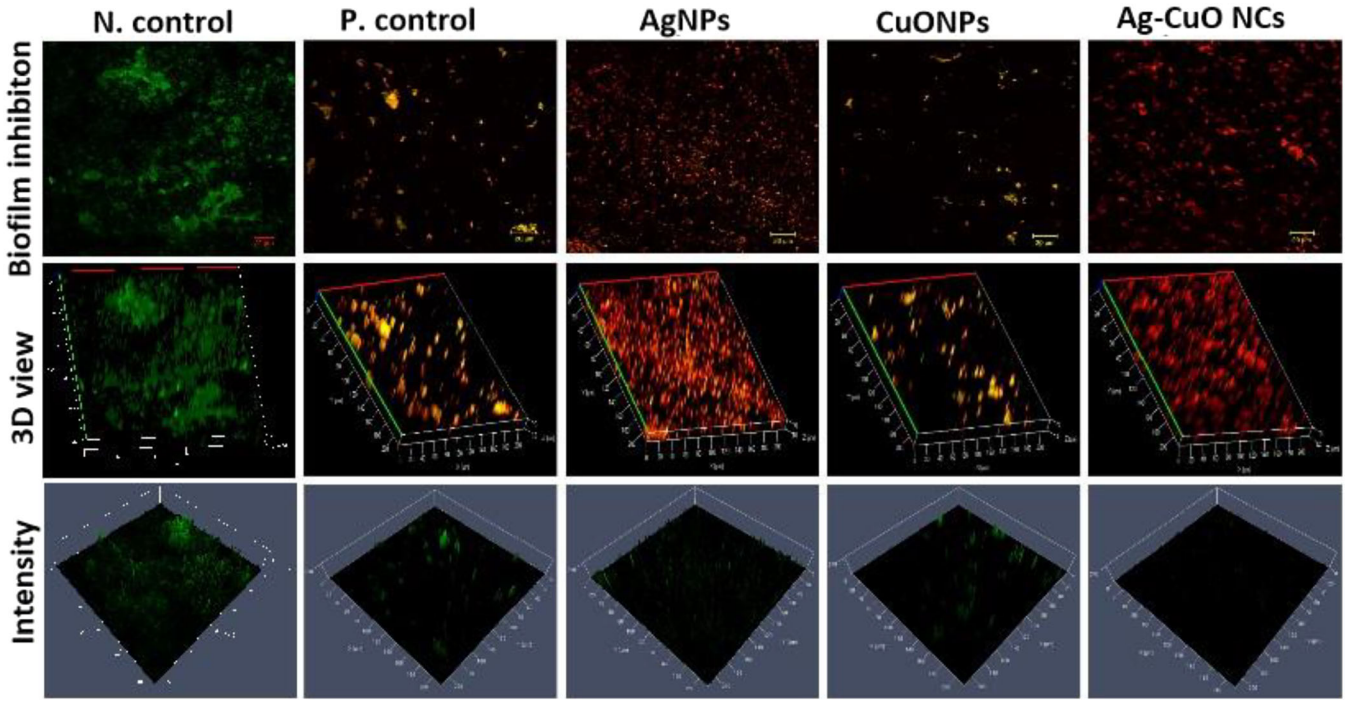


**FIGURE 13** CLSM image of *Staphylococcus aureus* biofilm formation treated with green fabricated AgNPs, CuONPs, and Ag-CuO NCs (100 μg/mL). Panel of images show the tree dimensional view of biofilm formed by control and treated cultures and their two-dimensional views with their respective intensity projections. Each experiment was performed using three independent cultures, and one representative data set is shown here. Scale bars = 50 μm.

directly through sulfur/phosphorus-containing proteins of the plasma membrane or bacterial cell wall, creating membrane holes and flowing out the cytoplasmic content of the cell that leads to bacterial cell death. Within the microbial cell, $Ag^{+}$ ions inhibit electron transport chain cytochromes, damage DNA, RNA, and ribosomes, and generate ROS, which appeared to be toxic to both bacterial and eukaryotic host cells.[76] The copper mechanism of action has previously been suggested as a result of copper ions attacking the outer membrane, breaching the cell wall, causing nucleic acids damage, and ultimately destroying the bacterial cell.[77] The minimum concentration (30–45 μg $mL^{-1}$) of CuO NPs exterminate 43.8% of *P. aeruginosa* biofilm.[78] The differential inhibitory effect may also be caused by several factors, which would include antimicrobial efficacy, NP size, penetration abilities, and physical and other chemical properties influencing the attraction between materials and biofilms.[79] The hydroxyapatite nanoparticles (nHAP) and green and chemical synthesized zinc oxide nanoparticles acted as antimicrobial agent against clinically isolated Gram-positive *S. aureus* and Gram-negative *E. coli*. Green synthesized nHAP-ZnO nanocomposites showed potent antibiofilm activity against *S. aureus* (52%) and *E. coli* (54%).[80]

## 3.5 | Analysis of AgNPs, CuONPs, and hybrid Ag-CuO NCs treated bacteria by FE-SEM

Biofilm formation stipulates the pathogens with a strong ability to invade the host, adapt, and modify its immediate environment. Therefore, the microbial population in a biofilm can withstand adverse environmental conditions while being less susceptibility to conventional antibiotics.[81] Biofilm inhibits antibacterial agent action in a number of different ways, including antimicrobial diffusion through the extracellular matrix, altered phenotype, slow cell growth, and the existence of persistent cells.[82] The green synthesized AgNPs, CuONPs, and hybrid Ag-CuO NCs were investigated for antibiofilm formation against *A. hydrophila*, *P. aeruginosa*, and *S. aureus*. The negative control (untreated) cells showed dense layer and bacterial cells adhered over the surface of the substrate. The positive control (streptomycin) treated biofilm structure showed eradicated and reduced surface attached cells. In *A. hydrophila*, the AgNPs, CuONPs, and hybrid Ag-CuO NCs caused significant loss of biofilm and cell growth as compared to the negative control (Figure 14). The significant antibiofilm results were also observed on *P. aeruginosa* and *S. aureus*. FE-SEM micrographs

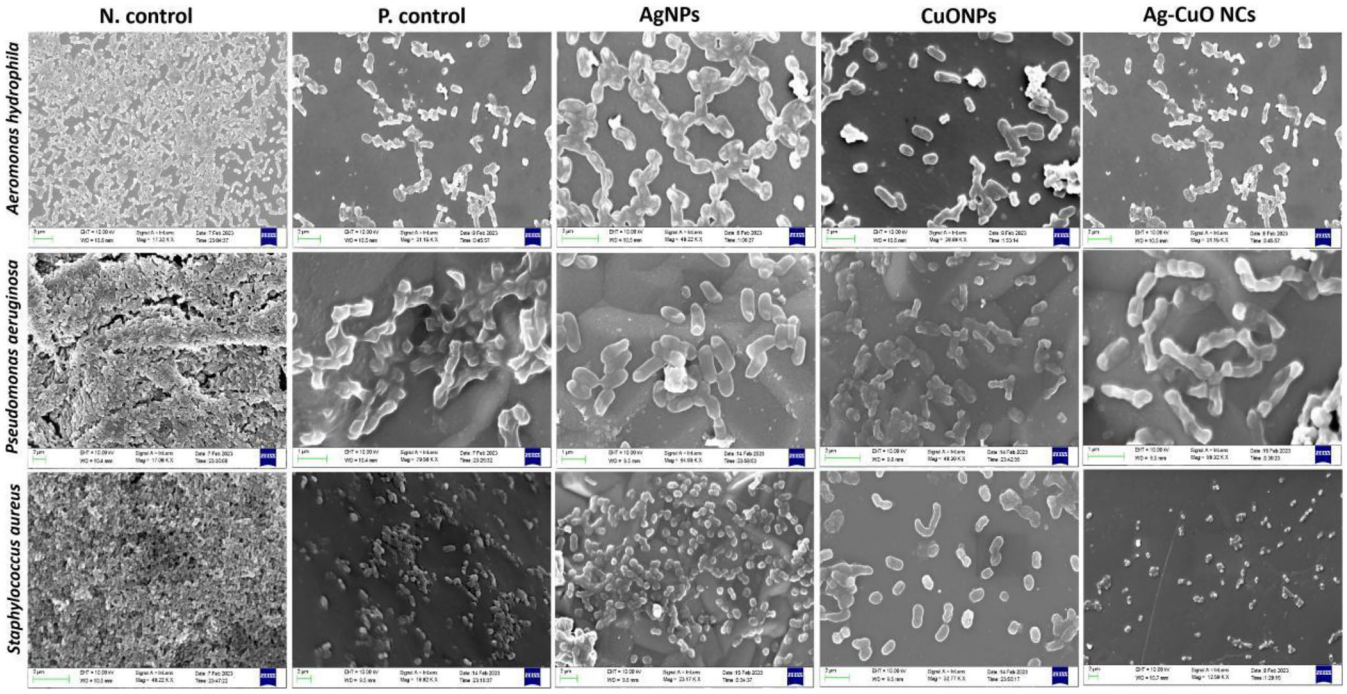


**FIGURE 14** Visualization of pathogens by field emission scanning electron microscopy analysis. The FE-SEM micrographs of green synthesized AgNPs, CuONPs, and hybrid Ag-CuO NCs on antibiofilm formation treated against *Aeromonas hydrophila*, *Pseudomonas aeruginosa*, and *Staphylococcus aureus*. Untreated cells as negative control and streptomycin used as the positive control.

demonstrated that the biofilm thickness and structural morphology alteration were obtained in all the three pathogenic microorganisms (Figure 14). From the experimental results, it is evident that the synthesized nanomaterials of this study altered the biofilm architecture and reduced the bacterial adhesion. It might be directly entangled toward the toxicity and pathogenicity, apart from EPS production.[83] The destructive effects of nanomaterial on the concentration, size, shape, and surface charge may affect the growth of cell and biofilm formation. Nanomaterials bind to multi-targeted sites simultaneously including DNA, lipid, plasmid, cell membrane, enzymes, and proteins.[84] The silver nanoparticle decorated with hydroxyapatite (HA@Ag) poriferous nanocomposites have showed potential antibacterial efficacy. The HA@Ag nanocomposites (100 μg/mL$^{-1}$) exhibited morphological alterations in bacterial cells due to interalization of nanocomposites.[85]

Antibacterial effect of AgNPs was excellent against pathogenic microorganisms, but the antibacterial mechanism of AgNPs has not been understood well.[86] The induced oxidative stress by AgNPs such as dissolution, aggregation, oxidation, and sulfidation are the main factors for the physicochemical transformation.[87] Bactericidal effect was based upon the electrostatic interaction between bacteria and NPs; thus, the positive charged NPs can easily bind with negatively charged bacterial membrane.[88] The AgNPs could damage the bacterial cell through enzymatic dysfunction, cellular protein inactivation, and DNA damage.[89] The core possible mechanism of antimicrobial efficiency is the dissolution of AgNPs by releasing $Ag^+$ ions, which could interact with sulfur-containing proteins in the bacterial cell wall, giving rise to compromised functionality.[90] *Turnera subulata* Sm. copper nanoparticles (TS-CuNPs) have showed an efficacious activity against pathogenic microorganisms, and the higher zone of inhibition was recorded at 75 μg/mL on account of structural changes in the cell wall (gram positive and gram negative) by the nanomaterial, resulting in cell death after cytoplasm degradation.[69] Similar reports have indicated that copper (Cu) attaches to the bacterial cell wall and causes bacterial structure dysfunction/disintegration. Latterly, Cu ions bind with DNA and disrupt enzymatic reaction leading to cell death.[2] Al-Zaqri et al.[48] reported that zirconium oxide nanoparticles ($ZrO_2$-NPs) were synthesized using *Wrightia tinctoria* leaf extract and demonstrated excellent antibacterial activity against Gram-positive and Gram-negative bacteria. $ZrO_2$-NPs displayed ROS-mediated cell death as a result of van der Waals force interaction with the cell wall by changing the membrane fluidity to facilitate cellular entry. The antibacterial mechanism of *Syzygium aromaticum* (Sa-AgNPs) was tested against *Salmonella typhimurium*, and the bacterial cells adsorb Sa-AgNPs through the bacterial

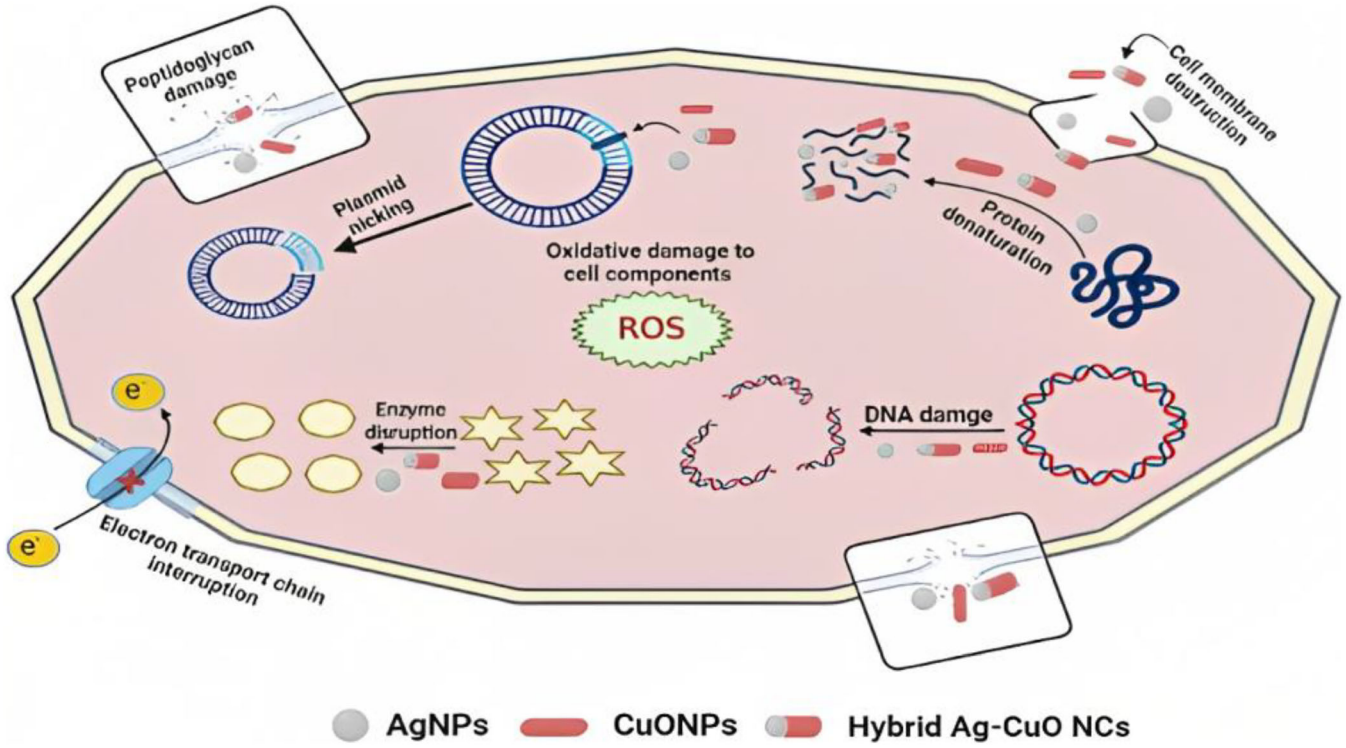


FIGURE 15 Plausible antibacterial mechanism of green synthesized AgNPs, CuONPs, and hybrid Ag-CuO NCs.

cytoplasm without rupturing the bacterial cell membrane (endocytosis), and bacterial cellular components were disrupted by oxidizing unsaturated fatty acids and ROS production.[91] The proposed mechanism of antibacterial potential of AgNPs, CuONPs, and Ag-CuO NCs is the generation of ROS from the surface of the NPs, resulting in oxidative stress to the bacterial strains via DNA breakage, enzyme disruption, cell membrane destruction, protein denaturation, peptidoglycan damage, and electron transport chain interruption as illustrated in Figure 15.

## 4 | CONCLUSION

Biofilms, as the thereabouts signal of bacterial growth, pose a major obstacle that traditional antimicrobial therapeutics have yet to surmount. It has raised concerns that protracted antibiotic usage may result in the emergence of MDR strains. Biofilm infections are highly resistant to current antimicrobial therapy, producing a substantial impact on global concern toward healthcare sector. Green fabricated AgNPs, CuONPs, and Ag-CuO NCs were characterized by fluorescence and Raman spectroscopy, FE-SEM coupled with EDX, and TG/DSC analysis to understand physicochemical characteristic nature of the nanoparticles (chemical interactions, surface topology, and thermal behavior). Green chemistry approach could be alternative to the conventional and synthetic antibiotics, in view of antimicrobial resistance. Green fabricated AgNPs, CuONPs, and Ag-CuO NCs elucidate inhibitory antibiofilm potency against pathogenic microorganisms. Furthermore, the present study of nanomaterials could be helpful in developing a prominent candidate for preventing biofilm-related disease outbreaks in aquaculture. Future studies will emphasize the complete removal of biofilm (EPX matrix) by enhancing therapeutic potential with diminished toxic effects and resistance capacity for further biological investigations.

## AUTHOR CONTRIBUTIONS

**Dinesh Babu Manikandan:** Investigation; methodology; data curation; writing—original draft. **Manikandan Arumugam:** Investigation; resources. **Ubais Abdul:** Methodology; resources. **Arun Sridhar:** Investigation; resources. **Zulhisyam Abdul Kari:** Editing; data curation; funding. **Guillermo Téllez-Isaías:** Editing; resources, Funding. **Thirumurugan Ramasamy:** Conceptualization; project administration; supervision; validation; visualization; writing—review and editing. All the authors contributed to the article and approved the final version.

## ACKNOWLEDGMENTS

The first author Dinesh Babu Manikandan would like to thank RUSA 2.0 for granting Research Associate, Biological Sciences, Department of Animal Science,

Bharathidasan University (Ref. No: 65-3 BDU/RUSA 2.0/TRP/BS/Date: 4/5/2022). The authors are gratefully thanking to UGC-SAP-DRS-II (F.3-9/2013[SAP-II]), Department of Science and Technology-Fund for Improvement of Science and Technology Infrastructure (DST-FIST)-Level I (stage II) (Ref. No. SR/FST/LSI-647/2015(C) Date.11.08.2016), and the Department of Science and Technology Promotion of University Research and Scientific Excellence (DST PURSE Phase II) (Ref. No. SR/PURSE PHASE 2/16(G) /& 16(C) Date. 21.02.2017) of the Department of Animal Science, Bharathidasan University, for the instrumental facility and the University Science Instrumentation Centre (USIC), Bharathidasan University, for providing confocal microscope facility DST-PURSE program (Phase 1) (Sanction Order No. SR/FT/LS-113/2009), fluorescence spectroscopy, and thermal characterization studies.

## CONFLICT OF INTEREST STATEMENT

The authors declare that they have no conflicts of interest.

## DATA AVAILABILITY STATEMENT

The data that support the findings of this study are available from the corresponding author upon reasonable request.

## REFERENCES

[1] M. Seong, D. G. Lee, *Microbiol. Res.* **2018**, *207*, 33.
[2] K. V. Tregubova, I. V. Yegorenkova, V. S. Grinev, A. S. Fomin, *Enzyme Microb. Technol.* **2023**, *164*, 110174.
[3] D. G. Hirpara, H. P. Gajera, *Appl. Organomet. Chem.* **2020**, *34*(3), e5407.
[4] C. Gu, Z. Wang, Y. Pan, S. Zhu, Z. Gu, *Adv. Mater.* **2023**, *35*(1), 2204397.
[5] S. Nayak, M. P. Bhat, A. C. Udayashankar, T. R. Lakshmeesha, N. Geetha, S. Jogaiah, *Appl. Organomet. Chem.* **2020**, *34*(4), e5567.
[6] M. Hamelian, M. M. Zangeneh, A. Amisama, K. Varmira, H. Veisi, *Appl. Organomet. Chem.* **2018**, *32*(9), e4458.
[7] P. Balashanmugam, M. D. Balakumaran, R. Murugan, K. Dhanapal, P. T. Kalaichelvan, *Microbiol. Res.* **2016**, *192*, 52.
[8] D. M. Ceballos, A. S. Young, J. G. Allen, A. J. Specht, V. T. Nguyen, J. A. Craig, M. Miller, T. F. Webster, *Int. J. Hyg. Environ. Health.* **2021**, *232*, 113687.
[9] Z. K. Zhasnakunov, A. C. Satyvaldiev, T. Doolotkeldieva, E. Omurzak, S. T. Bobusheva, Z. Kelgenbaeva, Z. Abdullaeva, *Mater. Res. Express.* **2018**, *5*(8), 085404.
[10] Y. H. Kim, D. K. Lee, H. G. Cha, C. W. Kim, Y. S. Kang, *J. Phys. Chem. C* **2007**, *111*(9), 3629.
[11] S. Mahboub, D. Zerrouki, A. Henni, *Appl. Organomet. Chem.* **2020**, *34*(12), e5956.
[12] M. Naseer, U. Aslam, B. Khalid, B. Chen, *Sci. Rep.* **2020**, *10*(1), 1.
[13] A. Ullah, Z. A. Mirani, S. Binbin, F. Wang, M. W. H. Chan, S. Aslam, L. Yonghong, N. Hasan, M. Naveed, S. Hussain, Z. Khatoon, *Process Biochem.* **2023**, *126*, 98.
[14] N. Chari, L. Felix, M. Davoodbasha, A. S. Ali, T. Nooruddin, *Biocatal. Agric. Biotechnol.* **2017**, *10*, 336.
[15] K. E. Jones, N. G. Patel, M. A. Levy, A. Storeygard, D. Balk, J. L. Gittleman, P. Daszak, *Nature* **2008**, *451*(7181), 990.
[16] N. Tharmalingam, R. Khader, B. B. Fuchs, E. Mylonakis, *Front. Microbiol.* **2019**, *10*, 1557.
[17] C. Y. Loo, R. Rohanizadeh, P. M. Young, D. Traini, R. Cavaliere, C. B. Whitchurch, W. H. J. Lee, *Agric. Food. Chem.* **2016**, *64*(12), 2513.
[18] A. Materazzi, D. Bottai, C. Campobasso, A. B. Klatt, N. Cesta, M. De Masi, A. Trampuz, A. Tavanti, M. Di Luca, *Int. J. Mol. Sci.* **2022**, *23*(23), 14514.
[19] B. Jena, S. S. Singh, S. K. Behera, S. Mishra, S. Chakrabortty, D. Meher, B. Mulia, S. K. Tripathy, R. Kumar, B. H. Jeon, C. S. Lundborg, *Environ. Res.* **2023**, *216*, 114700.
[20] M. A. Rather, D. Saha, S. Bhuyan, A. N. Jha, M. Mandal, *Microbiol. Res.* **2022**, *264*, 127173.
[21] I. Zmysłowska, K. Korzekwa, J. Szarek, *J. Comp. Pathol.* **2009**, *4*(141), 313.
[22] D. Stratev, O. A. Odeyemi, *J. Infect. Public Health.* **2016**, *9*(5), 535.
[23] A. Vikram, G. K. Jayaprakasha, P. R. Jesudhasan, S. D. Pillai, B. S. Patil, *J. Appl. Microbiol.* **2010**, *109*(2), 515.
[24] K. Lewis, *Nat. Rev. Microbiol.* **2007**, *5*(1), 48.
[25] S. Reddy, K. Kaur, P. Barathe, V. Shriram, M. Govarthanan, V. Kumar, *Microbiol. Res.* **2022**, *263*, 127135.
[26] S. Aghamohammad, M. Rohani, *Microbiol. Res.* **2022**, 127275.
[27] D. B. Manikandan, A. Sridhar, R. K. Sekar, B. Perumalsamy, S. Veeran, M. Arumugam, P. Karuppaiah, T. J. Ramasamy, *Environ. Chem. Eng.* **2021**, *9*(1), 104845.
[28] D. B. Manikandan, M. Arumugam, S. Veeran, A. Sridhar, R. Krishnasamy Sekar, B. Perumalsamy, T. Ramasamy, *Environ. Sci. Pollut. Res.* **2021**, *28*(26), 33927.
[29] D. B. Manikandan, M. Arumugam, A. Sridhar, B. Perumalsamy, T. Ramasamy, *Environ. Res.* **2023**, *228*, 115867.
[30] A. Dheilly, E. Soum-Soutéra, G. L. Klein, A. Bazire, C. Compère, D. Haras, A. Dufour, *Appl. Environ. Microbiol.* **2010**, *76*(11), 3452.
[31] J.E. Cassat, C.Y. Lee, M.S. Smeltzer, **2007**, 127–144.
[32] F. E. Ettadili, M. Azriouil, B. Chhaibi, F. Z. Ouatmane, O. T. Alaoui, F. Laghrib, A. Farahi, M. Bakasse, S. Lahrich, M. E. Mhammedi, *Food Chem.* **2023**, *2*, 100146.
[33] S. Patel, P. Patel, S. B. Undre, S. R. Pandya, M. Singh, S. Bakshi, *J. Mol. Liq.* **2016**, *213*, 304.
[34] Y. Wu, Y. Yang, Z. Zhang, Z. Wang, Y. Zhao, L. Sun, *Adv. Powder Technol.* **2018**, *29*(2), 407.
[35] S. Alamdari, M. Sasani Ghamsari, C. Lee, W. Han, H. H. Park, M. J. Tafreshi, H. Afarideh, M. H. M. Ara, *Appl. Sci.* **2020**, *10*(10), 3620.
[36] K. Anandalakshmi, J. Venugobal, V. Ramasamy, *Appl. Nanosci.* **2016**, *6*(3), 399.
[37] B. T. Sone, A. Diallo, X. G. Fuku, A. Gurib-Fakim, M. Maaza, *Arabian J. Chem.* **2020**, *13*(1), 160.
[38] R. M. Mohamed, F. A. Harraz, A. Shawky, *Ceram. Int.* **2014**, *40*(1), 2127.

[39] J. Yang, Z. Li, W. Zhao, C. Zhao, Y. Wang, X. Liu, *Mater. Lett.* **2014**, *120*, 16.

[40] H. Yao, X. Dong, H. Xiong, J. Liu, J. Zhou, Y. Ye, *Spectrochim. Acta, Part a* **2022**, *280*, 121464.

[41] S. Sang, D. Li, H. Zhang, Y. Sun, A. Jian, Q. Zhang, W. Zhang, *RSC Adv.* **2017**, *7*(35), 21618.

[42] A. Munoz-Escobar, Á.D.J. Ruíz-Baltazar, S.Y. Reyes-López, **2019**, *17*(3).

[43] A. Sridevi, B. Balraj, N. Senthilkumar, G. K. D. Venkatesan, *J. Supercond. Novel Magn.* **2020**, *33*(11), 3501.

[44] P. Singh, I. Mijakovic, *Biomedicines.* **2022**, *10*(3), 628.

[45] P. C. Nagajyothi, P. Muthuraman, T. V. M. Sreekanth, D. H. Kim, J. Shim, *Arabian J. Chem.* **2017**, *10*(2), 215.

[46] M. Rakibuddin, S. Mandal, R. Ananthakrishnan, *New J. Chem.* **2017**, *41*(3), 1380.

[47] S. Sampaio, J. C. Viana, *Adv. Nat. Sci.: Nanosci. Nanotechnol.* **2018**, *9*(4), 045002.

[48] N. Al-Zaqri, A. Muthuvel, M. Jothibas, A. Alsalme, F. A. Alharthi, V. Mohana, *Inorg. Chem. Commun.* **2021**, *127*, 108507.

[49] L. David, B. Moldovan, *Nanomaterials* **2020**, *10*(2), 202.

[50] S. Shrivastava, T. Bera, A. Roy, G. Singh, P. Ramachandrarao, D. Dash, *Nanotechnology* **2007**, *18*(22), 225103.

[51] W. Abdussalam-Mohammed, L. Mohamed, M. S. Abraheem, M. M. Mansour, A. M. Sherif, *Chemistry* **2023**, *5*(1), 54.

[52] Z. Qi, P. Xie, C. Yang, X. Xue, H. Chen, H. Zhou, H. Yuan, G. Yang, C. Wang, *Food Chem.* **2023**, *407*, 135122.

[53] X. Xie, H. Lei, D. Fan, *J. Mater. Sci. Technol.* **2023**, *144*, 198.

[54] O. Choi, Z. Hu, *Environ. Sci. Technol.* **2008**, *42*(12), 4583.

[55] M. E. Mouzahim, E. M. Eddarai, S. Eladaoui, A. Guenbour, A. Bellaouchou, A. Zarrouk, R. Boussen, *Food Chem.* **2023**, *410*, 135470.

[56] E. Sánchez-López, D. Gomes, G. Esteruelas, L. Bonilla, A. L. Lopez-Machado, R. Galindo, A. Cano, M. Espina, M. Ettcheto, A. Camins, A. M. Silva, *Nanomaterials* **2020**, *10*(2), 292.

[57] A. Plotniece, A. Sobolev, C. T. Supuran, F. Carta, F. Björkling, H. Franzyk, J. Yli-Kauhaluoma, K. Augustyns, P. Cos, L. De Vooght, M. Govaerts, *J. Enzyme Inhib. Med. Chem.* **2023**, *38*(1), 2155816.

[58] Y. N. Slavin, J. Asnis, U. O. Häfeli, H. Bach, *J. Nanobiotechnol.* **2017**, *15*(1), 1.

[59] D. S. Handayani, D. A. Saputra, S. D. Marliyana, *IOP Conf. Ser.: Mater. Sci. Eng.* **2019**, *578*, 012061.

[60] R. B. Asamoah, E. Annan, B. Mensah, P. Nbelayim, V. Apalangya, B. Onwona-Agyeman, A. Yaya, *Adv. Mater. Sci. Eng.* **2020**, *2020*, 1.

[61] M. Xu, H. Luo, H. Rong, S. Wu, Z. Zheng, B. Chen, *Int. J. Biol. Macromol.* **2023**, *231*, 123289.

[62] Z. Ni, M. Wan, G. Tang, L. Sun, *Polymer* **2022**, *14*(24), 5422.

[63] T. Manchanayake, A. Salleh, M. N. A. Amal, I. S. M. Yasin, M. Zamri-Saad, *Aquac. Rep.* **2023**, *28*, 101459.

[64] S. Park, H. H. Park, S. Y. Kim, S. J. Kim, K. Woo, G. Ko, *Appl. Environ. Microbiol.* **2014**, *80*(8), 2343.

[65] M. K. Joshi, H. R. Pant, H. J. Kim, J. H. Kim, C. S. Kim, *Colloids Surf., a* **2014**, *446*, 102.

[66] S. Huang, D. Ma, Z. Hu, Q. He, J. Zai, D. Chen, H. Sun, Z. Chen, Q. Qiao, M. Wu, X. Qian, *ACS Appl. Mater. Interfaces* **2017**, *9*(33), 27607.

[67] D. Prabina, T. R. Swaminathan, S. P. Mohandas, J. C. Anjana, K. Manjusha, P. G. Preena, *Arch. Microbiol.* **2023**, *205*, 41.

[68] M. K. D. Dueholm, M. Besteman, E. J. Zeuner, M. Riisgaard-Jensen, M. E. Nielsen, S. Z. Vestergaard, S. Heidelbach, N. S. Bekker, P. H. Nielsen, *Water Res.* **2023**, *229*, 119485.

[69] S. Cavalu, S. S. Elbaramawi, A. G. Eissa, M. F. Radwan, S. Ibrahim, T. E. S. Khafagy, B. S. Lopes, M. A. Ali, W. A. Hegazy, M. A. Elfaky, *Int. J. Mol. Sci.* **2022**, *23*(21), 13088.

[70] F. Martinez-Gutierrez, L. Boegli, A. Agostinho, E. M. Sánchez, H. Bach, F. Ruiz, G. James, *Biofouling* **2013**, *29*(6), 651.

[71] M. Eshed, J. Lellouche, A. Gedanken, E. Banin, *Adv. Funct. Mater.* **2014**, *24*(10), 1382.

[72] J. Jang, J. M. Lee, S. B. Oh, Y. Choi, H. S. Jung, J. Choi, *ACS Appl. Mater. Interfaces* **2020**, *12*(32), 35826.

[73] Y. K. Mohanta, K. Biswas, S. K. Jena, A. Hashem, E. F. Abd_Allah, T. K. Mohanta, *Front. Microbiol.* **2020**, *11*, 1143.

[74] M. Yazhiniprabha, B. Vaseeharan, A. Sonawane, A. Behera, *J. Photochem. Photobiol. B: Biol.* **2019**, *192*, 158.

[75] O. Gordon, T. V. Slenters, P. S. Brunetto, A. E. Villaruz, D. E. Sturdevant, M. Otto, R. Landmann, K. M. Fromm, *Antimicrob. Agents Chemother.* **2010**, *54*(10), 4208.

[76] A. Taglietti, C. R. Arciola, A. D'Agostino, G. Dacarro, L. Montanaro, D. Campoccia, L. Cucca, M. Vercellino, A. Poggi, P. Pallavicini, L. Visai, *Biomaterials* **2014**, *35*(6), 1779.

[77] J. Wu, Y. Wu, Y. Yuan, C. Xia, M. Saravanan, S. Shanmugam, A. Sabour, M. Alshiekheid, K. Brindhadevi, N. T. L. Chi, A. Pugazhendhi, *Food Chem. Toxicol.* **2022**, *168*, 113366.

[78] M. Agarwala, B. Choudhury, R. N. S. Yadav, *Indian J. Microbiol.* **2014**, *54*, 365.

[79] H. J. Park, H. Y. Kim, S. Cha, C. H. Ahn, J. Roh, S. Park, S. Kim, K. Choi, J. Yi, Y. Kim, J. Yoon, *Chemosphere* **2013**, *92*(5), 524.

[80] Z. Beyene, R. Ghosh, *Mater. Today Commun.* **2019**, *21*, 100612.

[81] A. Miškovská, M. Rabochová, J. Michailidu, J. Masák, A. Čejková, J. Lorinčík, O. Maťátková, *PLoS ONE* **2022**, *17*(8), e0272844.

[82] P. François, J. Schrenzel, F. Götz, *Int. J. Mol. Sci.* **2023**, *24*(6), 5218.

[83] S. Dutta Sinha, S. Chatterjee, P. K. Maiti, S. Tarafdar, S. P. Moulik, *Prog. Biomater.* **2017**, *6*, 27.

[84] B. Ahmed, F. Ameen, A. Rizvi, K. Ali, H. Sonbol, A. Zaidi, M. S. Khan, J. Musarrat, *ACS Omega* **2020**, *5*(14), 7861.

[85] T. O. Abolarinwa, D. J. Ajose, B. O. Oluwarinde, J. Fri, K. P. Montso, O. E. Fayemi, A. O. Aremu, C. N. Ateba, *Front. Microbiol.* **2022**, *13*.

[86] Z. Ni, X. Gu, Y. He, Z. Wang, X. Zou, Y. Zhao, L. Sun, *RSC Adv.* **2018**, *8*(73), 41722.

[87] S. Sánchez-Salcedo, A. García, A. González-Jiménez, M. Vallet-Regí, *Acta Biomater.* **2023**, *155*, 654.

[88] S. Kamat, M. Kumari, *Front. Microbiol.* **2023**, *14*, 16.

[89] J. Lin, F. Gulbagca, A. Aygun, R. N. E. Tiri, C. Xia, Q. Van Le, T. Gur, F. Sen, Y. Vasseghian, *Food Chem. Toxicol.* **2022**, *163*, 112972.

[90] M. Guzman, J. Dille, S. Godet, *Nanomed.: Nanotechnol., Biol. Med.* **2012**, *8*(1), 37.

[91] S. Makky, N. Rezk, A. S. Abdelsattar, A. H. Hussein, A. Eid, K. Essam, A. G. Kamel, M. S. Fayez, M. Azzam, M. M. Agwa, A. El-Shibiny, *Results Phys.* **2023**, *5*, 100686.

## SUPPORTING INFORMATION

Additional supporting information can be found online in the Supporting Information section at the end of this article.

**How to cite this article:** D. B. Manikandan, M. Arumugam, U. Abdul, A. Sridhar, Z. Abdul Kari, G. Téllez-Isaías, T. Ramasamy, *Appl Organomet Chem* **2023**, *37*(12), e7293. https://doi.org/10.1002/aoc.7293